Chapter 4

The Intensity-Dependent Refractive Index

The refractive index of many optical materials depends on the intensity of the light used to measure the refractive index. In this chapter, we examine some of the mathematical descriptions of the nonlinear refractive index and examine some of the physical processes that give rise to this effect. In the following chapter, we study the origin of optical nonlinearities in molecular systems, in Chapter 6 we study the intensity-dependent refractive index resulting from the resonance response of an atomic system, and in Chapter 7 we study some physical processes that result from the nonlinear refractive index.

4.1 Descriptions of the Intensity-Dependent Refractive Index

The refractive index of many materials can be described by the relation

$$n = n_0 + \bar{n}_2 \langle \tilde{E}^2 \rangle, \tag{4.1.1}$$

where n_0 represents the usual, weak-field refractive index and $\bar{n}_2$ is a new optical constant (sometimes called the second-order index of refraction) that gives the rate at which the refractive index increases with increasing optical intensity.* The angular brackets surrounding the quantity $\tilde{E}^2$ represent a time average. Thus, if the optical field is of the form

$$\tilde{E}(t) = E(\omega) e^{-i\omega t} + \text{c.c.} \tag{4.1.2}$$

so that

$$\langle \tilde{E}(t)^2 \rangle = 2E(\omega)E(\omega)^* = 2\left|E(\omega)\right|^2, \tag{4.1.3}$$

* We place a bar over the symbol n_2 to prevent confusion with a different definition of n_2, which is introduced in Eq. (4.1.15).

Nonlinear Optics. https://doi.org/10.1016/B978-0-12-811002-7.00013-8

we find that

$$n = n_0 + 2\bar{n}_2 \left| E(\omega) \right|^2. \tag{4.1.4}$$

The change in refractive index described by Eq. (4.1.1) or (4.1.4) is sometimes called the optical Kerr effect, by analogy with the traditional Kerr electrooptic effect, in which the refractive index of a material changes by an amount that is proportional to the square of the strength of an applied static electric field.

Of course, the interaction of a beam of light with a nonlinear optical medium can also be described in terms of the nonlinear polarization. The part of the nonlinear polarization that influences the propagation of a beam of frequency ω is

$$P^{\mathrm{NL}}(\omega) = 3\epsilon_0 \chi^{(3)}(\omega = \omega + \omega - \omega) \left| E(\omega) \right|^2 E(\omega). \tag{4.1.5}$$

For simplicity we are assuming here that the light is linearly polarized and are suppressing the tensor indices of $\chi^{(3)}$; the tensor nature of $\chi^{(3)}$ is addressed explicitly in the following sections. The total polarization of the material system is then described by

$$P^{\mathrm{TOT}}(\omega) = \epsilon_0 \chi^{(1)} E(\omega) + 3\epsilon_0 \chi^{(3)} \left| E(\omega) \right|^2 E(\omega) \equiv \epsilon_0 \chi_{\mathrm{eff}} E(\omega), \tag{4.1.6}$$

where we have introduced the effective susceptibility

$$\chi_{\mathrm{eff}} = \chi^{(1)} + 3\chi^{(3)} \left| E(\omega) \right|^2. \tag{4.1.7}$$

In order to relate the nonlinear susceptibility $\chi^{(3)}$ to the nonlinear refractive index n_2, we note that it is generally true that

$$n^2 = 1 + \chi_{\mathrm{eff}}, \tag{4.1.8}$$

and by introducing Eq. (4.1.4) on the left-hand side and Eq. (4.1.7) on the right-hand side of this equation, we find that

$$\left[n_0 + 2\bar{n}_2 \left| E(\omega) \right|^2 \right]^2 = 1 + \chi^{(1)} + 3\chi^{(3)} \left| E(\omega) \right|^2. \tag{4.1.9}$$

Correct to terms of order $|E(\omega)|^2$, this expression when expanded becomes $n_0^2 + 4n_0\bar{n}_2|E(\omega)|^2 = (1 + \chi^{(1)}) + [3\chi^{(3)}|E(\omega)|^2]$, which shows that the linear and nonlinear re-

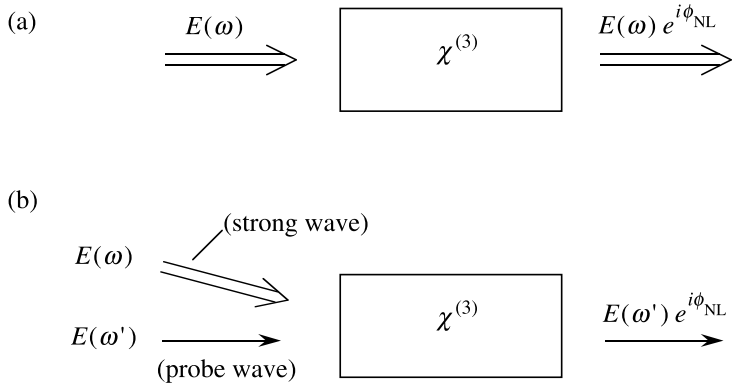

FIGURE 4.1.1: Two ways of measuring the intensity-dependent refractive index. In part (a), a strong beam of light modifies its own propagation, whereas in part (b), a strong beam of light influences the propagation of a weak beam.

fractive indices are related to the linear and nonlinear susceptibilities by

$$n_0 = \left(1 + \chi^{(1)}\right)^{1/2} \tag{4.1.10}$$

and

$$\bar{n}_2 = \frac{3\chi^{(3)}}{4n_0}. \tag{4.1.11}$$

The discussion just given has implicitly assumed that the refractive index is measured using a single laser beam, as shown in part (a) of Fig. 4.1.1. Another way of measuring the intensity-dependent refractive index is to use two separate beams, as illustrated in part (b) of the figure. Here the presence of the strong beam of amplitude $E(\omega)$ leads to a modification of the refractive index experienced by a weak probe wave of amplitude $E(\omega')$. The nonlinear polarization affecting the probe wave is given by

$$P^{\mathrm{NL}}(\omega') = 6\epsilon_0 \chi^{(3)}(\omega' = \omega' + \omega - \omega)\left|E(\omega)\right|^2 E(\omega'). \tag{4.1.12}$$

Note that the degeneracy factor (6) for this case is twice as large as that for the single-beam case of Eq. (4.1.5). In fact, for the two-beam case the degeneracy factor is equal to 6 even if ω' is equal to ω, because the probe beam is physically distinguishable from the strong pump beam owing to its different direction of propagation. The probe wave hence experiences a refractive index given by

$$n = n_0 + 2\bar{n}_2^{(\mathrm{cross})}\left|E(\omega)\right|^2, \tag{4.1.13}$$

where

$$\bar{n}_2^{(\text{cross})} = \frac{3\chi^{(3)}}{2n_0}. \tag{4.1.14}$$

Note that the nonlinear coefficient $\bar{n}_2^{(\text{cross})}$ describing cross-coupling effects is twice as large as the coefficient $\bar{n}_2$ of Eq. (4.1.11) which describes self-action effects. Hence, a strong wave affects the refractive index of a weak wave of the same frequency twice as much as it affects its own refractive index. This effect, for the case in which n_2 is positive, is known as weak-wave retardation (Chiao et al., 1966).

The quantity $\bar{n}_2$ is helpful for the conceptual understanding of nonlinear optical phenomena. However, in practice it is usually more convenient to use an alternative method for describing the intensity-dependent refractive index* by means of the quantity n_2 defined by the equation

$$n = n_0 + n_2 I, \tag{4.1.15}$$

where I denotes the time-averaged intensity of the optical field, given by

$$I = 2n_0'\epsilon_0 c\left|E(\omega)\right|^2. \tag{4.1.16}$$

Here we have expressed the refractive index in terms of its real and imaginary parts as $n = n' + in''$ and similarly for n_0 and n_2. Since the total refractive index n must be the same using either description of the nonlinear contribution, we see by comparing Eqs. (4.1.4) and (4.1.15) that

$$2\bar{n}_2\left|E(\omega)\right|^2 = n_2 I, \tag{4.1.17}$$

and thus that $\bar{n}_2$ and n_2 are related by

$$n_2 = \frac{\bar{n}_2}{n_0'\epsilon_0 c}, \tag{4.1.18}$$

where we have made use of Eq. (4.1.16). If Eq. (4.1.11) is introduced into this expression, we find that n_2 is related to $\chi^{(3)}$ by

$$n_2 = \frac{3}{4n_0 n_0'\epsilon_0 c}\chi^{(3)}. \tag{4.1.19}$$

This relation can be expressed numerically as

$$n_2\left(\frac{\text{m}^2}{\text{W}}\right) = \frac{283}{n_0 n_0'}\chi^{(3)}\left(\frac{\text{m}^2}{\text{V}^2}\right). \tag{4.1.20}$$

* For definiteness, we are treating the single-beam case of part (a) of Fig. 4.1.1. The extension to the two-beam case is straightforward.

TABLE 4.1.1: Typical values of the nonlinear refractive index[a].

Mechanism	n_2 (cm^2/W)	$\chi^{(3)}_{1111}$ (m^2/V^2)	Response time (sec)
Electronic polarization	10^{-16}	10^{-22}	10^{-15}
Molecular orientation	10^{-14}	10^{-20}	10^{-12}
Electrostriction	10^{-14}	10^{-20}	10^{-9}
Saturated atomic absorption	10^{-10}	10^{-16}	10^{-8}
Thermal effects	10^{-6}	10^{-12}	10^{-3}
Photorefractive effect[b]	(large)	(large)	(intensity-dependent)

[a] For linearly polarized light.
[b] The photorefractive effect often leads to a very strong nonlinear response. This response usually cannot be described in terms of a $\chi^{(3)}$ (or an n_2) nonlinear susceptibility, because the nonlinear polarization does not depend on the applied field strength in the same manner as the other mechanisms listed.

Nonlinear susceptibilities are sometimes quoted in gaussian units. Procedures for converting between the gaussian and SI units are presented in the appendix. One useful relation is the following:

$$n_2\left(\frac{\text{cm}^2}{\text{W}}\right) = \frac{12\pi^2}{n_0^2 c}10^7\chi^{(3)}(\text{esu}) = \frac{0.0395}{n_0^2}\chi^{(3)}(\text{esu}). \tag{4.1.21}$$

Some of the physical processes that can produce a nonlinear change in the refractive index are listed in Table 4.1.1, along with typical values of n_2, of $\chi^{(3)}$, and of the characteristic time scale for the nonlinear response to develop. Electronic polarization, molecular orientation, and thermal effects are discussed in the present chapter, saturated absorption is discussed in Chapter 7, electrostriction is discussed in Chapter 9, and the photorefractive effect is described in Chapter 11.

In Table 4.1.2 the experimentally measured values of the nonlinear susceptibility are presented for several materials. Some of the methods that are used to measure the nonlinear susceptibility have been reviewed by Hellwarth (1977). As an example of the use of Table 4.1.2, note that for fused silica the value of n_2 is approximately 3×10^{-16} $cm^2/W = 3 \times 10^{-20}$ m^2/W. Thus, a laser beam of intensity $I = 1$ $GW/cm^2 = 10$ TW/m^2 can produce a refractive index change of 3×10^{-7}. Even for As_2S_3 glass, the resulting change in refractive index is only approximately 700 times larger. Even though the fractional change in refractive index is usually very small, refractive index changes of this order of magnitude can lead to dramatic nonlinear optical effects (some of which are described in Chapter 7) for the case of phase-matched nonlinear optical interactions. Very recently, material systems have been identified for which the fractional change in refractive index can be of the order of unity. One such example is indium tin oxide, for which the change in index is 0.7 (Alam et al., 2016).

TABLE 4.1.2: Third-order nonlinear optical coefficients of various materials[a].

Material	n_0	$\chi^{(3)}$ (m^2/V^2)	n_2 (cm^2/W)	Comments and references[b]
Crystals				
Al_2O_3	1.8	3.1×10^{-22}	2.9×10^{-16}	1
CdS	2.34	9.8×10^{-20}	5.1×10^{-14}	1, 1.06 μm
Diamond	2.42	2.5×10^{-21}	1.3×10^{-15}	1
GaAs	3.47	1.4×10^{-18}	3.3×10^{-13}	15, 1.54 μm, $\beta = 10.2$ cm/GW
Ge	4.0	5.6×10^{-19}	9.9×10^{-14}	2, THG $\lvert\chi^{(3)}\rvert$
LiF	1.4	6.2×10^{-23}	9.0×10^{-17}	1
Si	3.4	2.8×10^{-18}	2.7×10^{-14}	15, 1.54 μm, $\beta = 0.79$ cm/GW
TiO_2	2.48	2.1×10^{-20}	9.4×10^{-15}	1
ZnSe	2.7	6.2×10^{-20}	3.0×10^{-14}	1, 1.06 μm
Glasses				
Fused silica	1.47	2.5×10^{-22}	3.2×10^{-16}	1
As_2S_3 glass	2.9	4.1×10^{-19}	2.4×10^{-13}	14
BK-7	1.52	2.8×10^{-22}	3.4×10^{-16}	1
BSC	1.51	5.0×10^{-22}	6.4×10^{-16}	1
Pb Bi gallate	2.3	2.2×10^{-20}	1.3×10^{-14}	4
SF-55	1.73	2.1×10^{-21}	2.0×10^{-15}	1
SF-59	1.953	4.3×10^{-21}	3.3×10^{-15}	1
Nanoparticles				
CdSSe in glass	1.5	1.4×10^{-20}	1.8×10^{-14}	3, nonres.
CS 3-68 glass	1.5	1.8×10^{-16}	2.3×10^{-10}	3, res.
Gold in glass	1.5	2.1×10^{-16}	2.6×10^{-10}	3, res.
Polymers				
Polydiacetylenes				
PTS		8.4×10^{-18}	$3. \times 10^{-12}$	5, nonres.
PTS		-5.6×10^{-16}	-2×10^{-10}	6, res.
9BCMU			2.7×10^{-18}	7, $\lvert n_2\rvert$, res.
4BCMU	1.56	-1.3×10^{-19}	-1.5×10^{-13}	8, nonres, $\beta = 0.01$ cm/MW
Liquids				
Acetone	1.36	1.5×10^{-21}	2.4×10^{-15}	9
Benzene	1.5	9.5×10^{-22}	1.2×10^{-15}	9
Carbon disulfide	1.63	3.1×10^{-20}	3.2×10^{-14}	9, $\tau = 2$ psec
CCl_4	1.45	1.1×10^{-21}	1.5×10^{-15}	9
Diiodomethane	1.69	1.5×10^{-20}	1.5×10^{-14}	9
Ethanol	1.36	5.0×10^{-22}	7.7×10^{-16}	9
Methanol	1.33	4.3×10^{-22}	6.9×10^{-16}	9
Nitrobenzene	1.56	5.7×10^{-20}	6.7×10^{-14}	9
Water	1.33	2.5×10^{-22}	4.1×10^{-16}	9

continued on next page

TABLE 4.1.2: (*continued.*)

Material	n_0	$\chi^{(3)}$ (m^2/V^2)	n_2 (cm^2/W)	Comments and references[b]
Other materials				
Air	1.0003	1.7×10^{-25}	5.0×10^{-19}	10
Ag		2.8×10^{-19}		2, THG $\lvert\chi^{(3)}\rvert$
Au		7.7×10^{-19}		2, THG $\lvert\chi^{(3)}\rvert$
		7.6×10^{-17}	$3.36i \times 10^{-14}$	16, 17, Z-scan, 6 ps, 630 nm
Vacuum	1	3.4×10^{-41}	1.0×10^{-34}	11
Cold atoms	1.0	7.1×10^{-8}	0.2	12, (EIT BEC)
Fluorescein dye in glass	1.5	$(2.8 + 2.8i) \times 10^{-8}$	$0.035(1 + i)$	13, $\tau = 0.1$ s
Indium tin oxide	0.4		1.1×10^{-10}	18, measured under ENZ conditions

[a] This table assumes the definition of the third-order susceptibility $\chi^{(3)}$ used in this book, as given for instance by Eq. (1.1.2) or by Eq. (1.3.21). This definition is consistent with that introduced by N. Bloembergen (*Nonlinear Optics*, Benjamin, New York, 1964). Some workers use an alternative definition which renders their values four times smaller. In compiling this table we have converted the literature values when necessary to the present definition.

[b] References for Table 4.1.2: (1) L.L. Chase and E.W. Van Stryland, Section 8.1 of *CRC Handbook of Laser Science and Technology*, CRC Press, Boca Raton, FL, 1995; (2) N. Bloembergen et al., *Opt. Commun.* 1, 195 (1969); (3) E.M. Vogel et al., *Phys. Chem. Glasses* 32, 231 (1991); (4) D.W. Hall et al., *Appl. Phys. Lett.* 54, 1293 (1989); (5) B.L. Lawrence et al., *Electron. Lett.* 30, 447 (1994); (6) G.M. Carter et al., *Appl. Phys. Lett*, 47, 457 (1985); (7) S. Molyneux, A.K. Kar, B.S. Wherrett, T.L. Axon, and D. Bloor, *Opt. Lett.* 18, 2093 (1993); (8) J.E. Erlich et al., *J. Mod. Opt.* 40, 2151 (1993); (9) R.L. Sutherland, *Handbook of Nonlinear Optics*, Chapter 8, Marcel Dekker, Inc., New York, 1996; (10) D.M. Pennington et al., *Phys. Rev. A* 39, 3003 (1989); (11) H. Euler and B. Kockel, *Naturwiss Enschaften* 23, 246 (1935); (12) L.V. Hau et al., *Nature* 397, 594 (1999); (13) M.A. Kramer, W.R. Tompkin, and R.W. Boyd, *Phys. Rev. A* 34, 2026 (1986); (14) R.E. Slusher et al., *J. Opt. Soc. Am. B* 21, 1146 (2004); (15) M. Dinu et al., *Appl. Phys. Lett.* 82, 2954 (2003); (16) N. Rotenberg et al., *Phys. Rev. B* 75, 155426 (2007); (17) the subtleties involved in determining the nonlinear coefficients of gold are described in R.W. Boyd et al., *Optics Commun.* 326, 74 (2014); (18) M.Z. Alam, I. De Leon, and R.W. Boyd, *Science* 352, 795 (2016).

4.2 Tensor Nature of the Third-Order Susceptibility

The third-order susceptibility $\chi^{(3)}_{ijkl}$ is a fourth-rank tensor, and thus is described in terms of 81 separate elements. For crystalline solids with low symmetry, all 81 of these elements are independent and can be nonzero (Butcher, 1965). However, for materials possessing a higher degree of spatial symmetry, the number of independent elements is very much reduced; as we show below, there are only three independent elements for an isotropic material.

Let us see how to determine the tensor nature of the third-order susceptibility for the case of an isotropic material such as a glass, a liquid, or a vapor. We begin by considering the general case in which the applied frequencies are arbitrary, and we represent the susceptibility as $\chi_{ijkl} \equiv \chi^{(3)}_{ijkl}(\omega_4 = \omega_1 + \omega_2 + \omega_3)$. Since each of the coordinate axes must be equivalent in an isotropic material, it is clear that the susceptibility possesses the following symmetry properties:

$$\chi_{1111} = \chi_{2222} = \chi_{3333}, \tag{4.2.1a}$$

$$\chi_{1122} = \chi_{1133} = \chi_{2211} = \chi_{2233} = \chi_{3311} = \chi_{3322}, \tag{4.2.1b}$$

$$\chi_{1212} = \chi_{1313} = \chi_{2323} = \chi_{2121} = \chi_{3131} = \chi_{3232}, \tag{4.2.1c}$$

$$\chi_{1221} = \chi_{1331} = \chi_{2112} = \chi_{2332} = \chi_{3113} = \chi_{3223}. \tag{4.2.1d}$$

One can also see that the 21 elements listed are the only nonzero elements of $\chi^{(3)}$, because these are the only elements that possess the property that any cartesian index (1, 2, or 3) that appears at least once appears an even number of times. An index cannot appear an odd number of times, because, for example, χ_{1222} would give the response in the $\hat{x}_1$ direction due to a field applied in the $\hat{x}_2$ direction. This response must vanish in an isotropic material, because there is no reason why the response should be in the $+\hat{x}_1$ direction rather than in the $-\hat{x}_1$ direction.

The four types of nonzero elements appearing in the four equations (4.2.1) are not independent of one another and, in fact, are related by the equation

$$\chi_{1111} = \chi_{1122} + \chi_{1212} + \chi_{1221}. \tag{4.2.2}$$

One can deduce this result by requiring that the predicted value of the nonlinear polarization be the same when calculated in two different coordinate systems that are rotated with respect to each other by an arbitrary amount. A rotation of 45 degrees about the $\hat{x}_3$ axis is a convenient choice for deriving this relation. The results given by Eqs. (4.2.1) and (4.2.2) can be used to express the nonlinear susceptibility in the compact form

$$\chi_{ijkl} = \chi_{1122}\delta_{ij}\delta_{kl} + \chi_{1212}\delta_{ik}\delta_{jl} + \chi_{1221}\delta_{il}\delta_{jk}. \tag{4.2.3}$$

This form shows that the third-order susceptibility has three independent elements for the general case in which the field frequencies are arbitrary.

Let us first specialize this result to the case of third-harmonic generation, where the frequency dependence of the susceptibility is taken as $\chi_{ijkl}(3\omega = \omega + \omega + \omega)$. As a consequence of the intrinsic permutation symmetry of the nonlinear susceptibility, the elements of the susceptibility tensor are related by $\chi_{1122} = \chi_{1212} = \chi_{1221}$ and thus Eq. (4.2.3) becomes

$$\chi_{ijkl}(3\omega = \omega + \omega + \omega) = \chi_{1122}(3\omega = \omega + \omega + \omega)(\delta_{ij}\delta_{kl} + \delta_{ik}\delta_{jl} + \delta_{il}\delta_{jk}). \tag{4.2.4}$$

Hence, there is only one independent element of the susceptibility tensor describing third-harmonic generation.

We next apply the result given in Eq. (4.2.3) to the nonlinear refractive index, that is, we consider the choice of frequencies given by $\chi_{ijkl}(\omega = \omega + \omega - \omega)$. For this choice of frequencies, the condition of intrinsic permutation symmetry requires that χ_{1122} be equal to χ_{1212}, and hence χ_{ijkl} can be represented by

$$\begin{aligned}\chi_{ijkl}(\omega = \omega + \omega - \omega) &= \chi_{1122}(\omega = \omega + \omega - \omega) \\ &\times (\delta_{ij}\delta_{kl} + \delta_{ik}\delta_{jl}) + \chi_{1221}(\omega = \omega + \omega - \omega)(\delta_{il}\delta_{jk}).\end{aligned} \tag{4.2.5}$$

The nonlinear polarization leading to the nonlinear refractive index is given in terms of the nonlinear susceptibility by (see also Eq. (1.3.21))

$$P_i(\omega) = 3\epsilon_0 \sum_{jkl} \chi_{ijkl}(\omega = \omega + \omega - \omega) E_j(\omega) E_k(\omega) E_l(-\omega). \tag{4.2.6}$$

If we introduce Eq. (4.2.5) into this equation, we find that

$$P_i = 6\epsilon_0 \chi_{1122} E_i(\mathbf{E} \cdot \mathbf{E}^*) + 3\epsilon_0 \chi_{1221} E_i^*(\mathbf{E} \cdot \mathbf{E}). \tag{4.2.7}$$

This equation can be written entirely in vector form as

$$\mathbf{P} = 6\epsilon_0 \chi_{1122}(\mathbf{E} \cdot \mathbf{E}^*)\mathbf{E} + 3\epsilon_0 \chi_{1221}(\mathbf{E} \cdot \mathbf{E})\mathbf{E}^*. \tag{4.2.8}$$

Following the notation of Maker and Terhune (1965) (see also Maker et al., 1964), we introduce the coefficients

$$A = 6\chi_{1122} \qquad (\text{or } A = 3\chi_{1122} + 3\chi_{1212}) \tag{4.2.9a}$$

and

$$B = 6\chi_{1221}, \tag{4.2.9b}$$

in terms of which the nonlinear polarization of Eq. (4.2.8) can be written as

$$\mathbf{P} = \epsilon_0 A(\mathbf{E} \cdot \mathbf{E}^*)\mathbf{E} + \tfrac{1}{2}\epsilon_0 B(\mathbf{E} \cdot \mathbf{E})\mathbf{E}^*. \tag{4.2.10}$$

We see that the nonlinear polarization consists of two contributions. These contributions have very different physical characters, since the first contribution has the vector nature of $\mathbf{E}$, whereas the second contribution has the vector nature of $\mathbf{E}^*$. Thus, for example, for circularly polarized light, the first contribution produces a nonlinear polarization with the same handedness as $\mathbf{E}$, whereas the second contribution produces a nonlinear polarization with the opposite handedness. The consequences of this behavior on the propagation of a beam of light through a nonlinear optical medium are described below.

The origin of the different physical characters of the two contributions to $\mathbf{P}$ can be understood in terms of the energy level diagrams shown in Fig. 4.2.1. Here part (a) illustrates one-photon-resonant contributions to the nonlinear coupling. We will show in Eq. (4.3.14) that processes of this sort contribute only to the coefficient A. Part (b) of the figure illustrates two-photon-resonant processes, which in general contribute to both the coefficients A and B (see Eqs. (4.3.13) and (4.3.14)). However, under certain circumstances, such as those described later in connection with Fig. 7.2.9, two-photon-resonant processes contribute only to the coefficient B.

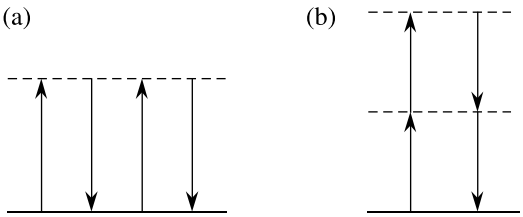

FIGURE 4.2.1: Diagrams (a) and (b) represent the resonant contributions to the nonlinear coefficients A and B, respectively.

For some purposes, it is useful to describe the nonlinear polarization not by Eq. (4.2.10) but rather in terms of an effective linear susceptibility defined by means of the relationship

$$P_i = \sum_j \epsilon_0 \chi_{ij}^{(\text{eff})} E_j. \tag{4.2.11}$$

Then, as can be verified by direct substitution, Eqs. (4.2.10) and (4.2.11) lead to identical predictions for the nonlinear polarization if the effective linear susceptibility is given by

$$\chi_{ij}^{(\text{eff})} = \epsilon_0 A'(\mathbf{E}\cdot\mathbf{E}^*)\delta_{ij} + \tfrac{1}{2}\epsilon_0 B'(E_i E_j^* + E_i^* E_j), \tag{4.2.12a}$$

where

$$A' = A - \tfrac{1}{2}B = 6\chi_{1122} - 3\chi_{1221} \tag{4.2.12b}$$

and

$$B' = B = 6\chi_{1221}. \tag{4.2.12c}$$

The results given in Eq. (4.2.10) or in Eqs. (4.2.12) show that the nonlinear susceptibility tensor describing the nonlinear refractive index of an isotropic material possesses only two independent elements. The relative magnitude of these two coefficients depends on the nature of the physical process that produces the optical nonlinearity. For some of the physical mechanisms leading to a nonlinear refractive index, these ratios are given by

$$B/A = 6, \quad B'/A' = -3 \quad \text{for molecular orientation,} \tag{4.2.13a}$$

$$B/A = 1, \quad B'/A' = 2 \quad \text{for nonresonant electronic response,} \tag{4.2.13b}$$

$$B/A = 0, \quad B'/A' = 0 \quad \text{for electrostriction.} \tag{4.2.13c}$$

These conclusions will be justified in the discussion that follows; see especially Eq. (4.4.37) for the case of molecular orientation, Eq. (4.3.14) for nonresonant electronic response of bound electrons, and Eq. (9.2.15) for electrostriction. Note also that A is equal to B by definition whenever the Kleinman symmetry condition is valid.

The trace of the effective susceptibility is given by

$$\mathrm{Tr}\,\chi_{ij} \equiv \sum_i \chi_{ii} = (3A' + B')\mathbf{E}\cdot\mathbf{E}^*. \tag{4.2.14}$$

Hence, $\mathrm{Tr}\,\chi_{ij}$ vanishes for the molecular orientation mechanism. This result can be understood from the point of view that molecular orientation does not add any "additional polarizability," it simply redistributes the amount that is present among different tensor components. For the resonant response of an atomic transition, the ratio of B to A depends upon the angular momentum quantum numbers of the two atomic levels. Formulas for A and B for such a case have been presented by Saikan and Kiguchi (1982).

4.2.1 Propagation through Isotropic Nonlinear Media

Let us next consider the propagation of a beam of light through a material whose nonlinear optical properties are described by Eq. (4.2.10). As we show below, only linearly or circularly polarized light is transmitted through such a medium with its state of polarization unchanged. When elliptically polarized light propagates through such a medium, the orientation of the polarization ellipse rotates as a function of propagation distance as a consequence of the nonlinear interaction.

Let us consider a beam of arbitrary polarization propagating in the positive z direction. The electric field vector of such a beam can always be decomposed into a linear combination of left- and right-hand circular components as

$$\mathbf{E} = E_+\hat{\boldsymbol{\sigma}}_+ + E_-\hat{\boldsymbol{\sigma}}_-, \tag{4.2.15}$$

where the circular-polarization unit vectors are illustrated in Fig. 4.2.2 and are defined by

$$\hat{\boldsymbol{\sigma}}_\pm = \frac{\hat{\mathbf{x}} \pm i\hat{\mathbf{y}}}{\sqrt{2}}. \tag{4.2.16}$$

By convention, $\hat{\boldsymbol{\sigma}}_+$ corresponds to left-hand circular and $\hat{\boldsymbol{\sigma}}_-$ to right-hand circular polarization (for a beam propagating in the positive z direction).

We now introduce the decomposition (4.2.15) into Eq. (4.2.10). We find, using the identities

$$\hat{\boldsymbol{\sigma}}_\pm^* = \hat{\boldsymbol{\sigma}}_\mp, \qquad \hat{\boldsymbol{\sigma}}_\pm \cdot \hat{\boldsymbol{\sigma}}_\pm = 0, \qquad \hat{\boldsymbol{\sigma}}_\pm \cdot \hat{\boldsymbol{\sigma}}_\mp = 1,$$

that the products $\mathbf{E}^*\cdot\mathbf{E}$ and $\mathbf{E}\cdot\mathbf{E}$ become

$$\begin{aligned}\mathbf{E}^*\cdot\mathbf{E} &= (E_+^*\hat{\boldsymbol{\sigma}}_+^* + E_-^*\hat{\boldsymbol{\sigma}}_-^*)\cdot(E_+\hat{\boldsymbol{\sigma}}_+ + E_-\hat{\boldsymbol{\sigma}}_-) = E_+^*E_+ + E_-^*E_- \\ &= |E_+|^2 + |E_-|^2\end{aligned}$$

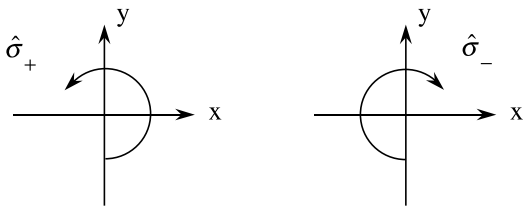

FIGURE 4.2.2: The $\hat{\boldsymbol{\sigma}}_+$ and $\hat{\boldsymbol{\sigma}}_-$ circular polarizations.

and

$$\mathbf{E}\cdot\mathbf{E} = (E_+\hat{\boldsymbol{\sigma}}_+ + E_-\hat{\boldsymbol{\sigma}}_-)\cdot(E_+\hat{\boldsymbol{\sigma}}_+ + E_-\hat{\boldsymbol{\sigma}}_-) = E_+E_- + E_-E_+ = 2E_+E_-,$$

so Eq. (4.2.10) can be written as

$$\mathbf{P}^{\mathrm{NL}} = \epsilon_0 A\big(|E_+|^2 + |E_-|^2\big)\mathbf{E} + \epsilon_0 B(E_+E_-)\mathbf{E}^*. \tag{4.2.17}$$

If we now represent $\mathbf{P}_{\mathrm{NL}}$ in terms of its circular components as

$$\mathbf{P}^{\mathrm{NL}} = P_+\hat{\boldsymbol{\sigma}}_+ + P_-\hat{\boldsymbol{\sigma}}_-, \tag{4.2.18}$$

we find that the coefficient P_+ is given by

$$\begin{aligned} P_+ &= \epsilon_0 A\big(|E_+|^2 + |E_-|^2\big)E_+ + \epsilon_0 B(E_+E_-)E_-^* \\ &= \epsilon_0 A\big(|E_+|^2 + |E_-|^2\big)E_+ + \epsilon_0 B|E_-|^2E_+ \\ &= \epsilon_0 A|E_+|^2E_+ + \epsilon_0(A+B)|E_-|^2E_+ \end{aligned} \tag{4.2.19a}$$

and similarly that

$$P_- = \epsilon_0 A|E_-|^2E_- + \epsilon_0(A+B)|E_+|^2E_-. \tag{4.2.19b}$$

These results can be summarized as

$$P_\pm \equiv \epsilon_0\chi_\pm^{\mathrm{NL}}E_\pm, \tag{4.2.20a}$$

where we have introduced the effective nonlinear susceptibilities

$$\chi_\pm^{\mathrm{NL}} = A|E_\pm|^2 + (A+B)|E_\mp|^2. \tag{4.2.20b}$$

The expressions (4.2.15) and (4.2.18) for the field and nonlinear polarization are now introduced into the wave equation,

$$\nabla^2\mathbf{E}(z,t) = \frac{\epsilon^{(1)}}{c^2}\frac{\partial^2\mathbf{E}(z,t)}{\partial t^2} + \frac{1}{\epsilon_0 c^2}\frac{\partial^2}{\partial t^2}\mathbf{P}^{\mathrm{NL}}, \tag{4.2.21}$$

where $\tilde{\mathbf{E}}(z,t) = \mathbf{E}\exp(-i\omega t) + \text{c.c.}$ and $\tilde{\mathbf{P}}(z,t) = \mathbf{P}\exp(-i\omega t) + \text{c.c.}$ We next decompose Eq. (4.2.21) into its $\hat{\boldsymbol{\sigma}}_+$ and $\hat{\boldsymbol{\sigma}}_-$ components. Since, according to Eq. (4.2.20a), $P_\pm$ is proportional to $E_\pm$, the two terms on the right-hand side of the resulting equation can be combined into a single term, so the wave equation for each circular component becomes

$$\nabla^2 \tilde{E}_\pm(z,t) = \frac{\epsilon_\pm^{(\text{eff})}}{c^2}\frac{\partial^2 \tilde{E}_\pm(z,t)}{\partial t^2}, \tag{4.2.22a}$$

where

$$\epsilon_\pm^{(\text{eff})} = \epsilon^{(1)} + \chi_\pm^{\text{NL}}. \tag{4.2.22b}$$

This equation possesses solutions of the form of plane waves propagating with the phase velocity $c/n^\pm$, where $n_\pm = [\epsilon_\pm^{(\text{eff})}]^{1/2}$. Letting $n_0^2 = \epsilon^{(1)}$, we find that

$$\begin{aligned} n_\pm^2 &= n_0^2 + \chi_\pm^{\text{NL}} = n_0^2 + \left[A|E_\pm|^2 + (A+B)|E_\mp|^2\right] \\ &= n_0^2\left(1 + \frac{1}{n_0^2}\left[A|E_\pm|^2 + (A+B)|E_\mp|^2\right]\right), \end{aligned}$$

and thus, noting that the second term in the last expression is much smaller than the first, that

$$n_\pm \simeq n_0 + \frac{1}{2n_0}\left[A|E_\pm|^2 + (A+B)|E_\mp|^2\right]. \tag{4.2.23}$$

We see that the left- and right-circular components of the beam propagate with different phase velocities. The difference in their refractive indices is given by

$$\Delta n \equiv n_+ - n_- = \frac{B}{2n_0}\left(|E_-|^2 - |E_+|^2\right). \tag{4.2.24}$$

Note that this difference depends upon the value of the coefficient B but not that of the coefficient A. Since the left- and right-hand circular components propagate with different phase velocities, the polarization ellipse of the light will rotate as a function of propagation distance within the medium.*

In order to determine the angle of rotation, we express the field amplitude as

$$\begin{aligned} E(z) &= E_+\hat{\boldsymbol{\sigma}}_+ + E_-\hat{\boldsymbol{\sigma}}_- = A_+e^{in_+\omega z/c}\hat{\boldsymbol{\sigma}}_+ + A_-e^{in_-\omega z/c}\hat{\boldsymbol{\sigma}}_- \\ &= \left(A_+e^{i(1/2)\Delta n\omega z/c}\hat{\boldsymbol{\sigma}}_+ + A_-e^{-i(1/2)\Delta n\omega z/c}\hat{\boldsymbol{\sigma}}_-\right)e^{i(1/2)(n_+ + n_-)\omega z/c}. \end{aligned} \tag{4.2.25}$$

We now introduce the mean propagation constant $k_m = \frac{1}{2}(n_+ + n_-)\omega/c$ and the angle

$$\theta = \tfrac{1}{2}\Delta n\frac{\omega}{c}z, \tag{4.2.26a}$$

* Recall that a similar effect occurs in the linear optics of optically active materials.

in terms of which Eq. (4.2.25) becomes

$$\mathbf{E}(z) = \left(A_+\hat{\boldsymbol{\sigma}}_+ e^{i\theta} + A_-\hat{\boldsymbol{\sigma}}_- e^{-i\theta}\right)e^{ik_m z}. \tag{4.2.26b}$$

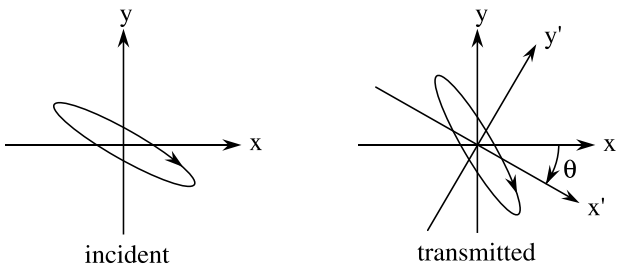

FIGURE 4.2.3: Polarization ellipses of the incident and transmitted waves.

As illustrated in Fig. 4.2.3, this equation describes a wave whose polarization ellipse is the same as that of the incident wave but rotated through the angle θ (measured clockwise in the xy plane, in conformity with the sign convention for rotation angles in optical activity). This conclusion can be demonstrated by noting that

$$\hat{\boldsymbol{\sigma}}_\pm e^{\pm i\theta} = \frac{\hat{x}' \pm i\,\hat{y}'}{\sqrt{2}}, \tag{4.2.27}$$

where $\hat{\mathbf{x}}'$ and $\hat{\mathbf{y}}'$ are polarization unit vectors in a new coordinate system—that is,

$$x' = x\cos\theta - y\sin\theta, \tag{4.2.28a}$$

$$y' = x\sin\theta + y\cos\theta. \tag{4.2.28b}$$

Measurement of the rotation angle θ provides a sensitive method for determining the nonlinear coefficient B (see also Eqs. (4.2.24) and (4.2.26a)).

As mentioned above, there are two cases in which the polarization ellipse does not rotate. One case is that of circularly polarized light. In this case only one of the $\hat{\sigma}_\pm$ components is present, and we see from Eq. (4.2.23) that the change in refractive index is given by

$$\delta n_{\text{circular}} = \frac{1}{2n_0}A|E|^2, \tag{4.2.29}$$

which clearly depends on the coefficient A but not on the coefficient B. The other case in which there is no rotation is that of linearly polarized light. Since linearly polarized light is a combination of equal amounts of left- and right-hand circular components (i.e., $|E_-|^2 = |E_+|^2$), we see directly from Eq. (4.2.24) that the index difference Δn vanishes. If we let E denote the

total field amplitude of the linearly polarized radiation, so that $|E|^2 = 2|E_+|^2 = 2|E_-|^2$, we find from Eq. (4.2.23) that for linearly polarized light the change in refractive index is given by

$$\delta n_{\text{linear}} = \frac{1}{2n_0}\left(A + \tfrac{1}{2}B\right)|E|^2. \tag{4.2.30}$$

Note that this change depends on the coefficients $A = 6\chi_{1122}$ and $B = 6\chi_{1221}$ as $A + \frac{1}{2}B$, which according to Eqs. (4.2.2) and (4.2.9) is equal to $3\chi_{1111}$. We see from Eqs. (4.2.29) and (4.2.30) that, for the usual case in which A and B have the same sign, linearly polarized light experiences a larger nonlinear change in refractive index than does circularly polarized light. In general the relative change in refractive index, $\delta n_{\text{linear}}/\delta n_{\text{circular}}$, is equal to $1 + B/2A$, which for the mechanisms described after Eq. (4.2.10) becomes

$$\frac{\delta n_{\text{linear}}}{\delta n_{\text{circular}}} = \begin{cases} 4 & \text{for molecular orientation,} \\ \frac{3}{2} & \text{for nonresonant electronic nonlinearities,} \\ 1 & \text{for electrostriction.} \end{cases}$$

For the case of two laser beams counterpropagating through a nonlinear material, the theoretical analysis is far more complex than that just presented for the single-beam situation, and a variety of additional phenomena can occur, including polarization bistability and polarization instabilities including chaos. These effects have been described theoretically by Gaeta et al. (1987) and have been observed experimentally by Gauthier et al. (1988, 1990).

4.3 Nonresonant Electronic Nonlinearities

Nonresonant electronic nonlinearities occur as the result of the nonlinear response of bound electrons to an applied optical field. This nonlinearity usually is not particularly large ($\chi^{(3)} \sim 10^{-22}$ m^2/V^2 is typical) but is of considerable importance because it is present in all dielectric materials. Furthermore, recent work has shown that certain organic nonlinear optical materials (such as polydiacetylene) can have nonresonant third-order susceptibilities as large as 10^{-17} m^2/V^2 as a consequence of the response of delocalized π electrons.

Nonresonant electronic nonlinearities are extremely fast, since they involve only virtual processes. The characteristic response time of this process is the time required for the electron cloud to become distorted in response to an applied optical field. This response time can be estimated as the orbital period of the electron in its motion about the nucleus, which according to the Bohr model of the atom is given by

$$\tau = 2\pi a_0/v,$$

where $a_0 = 0.5 \times 10^{-10}$ m is the Bohr radius of the atom and $v \simeq c/137$ is a typical electronic velocity. We hence find that $\tau \simeq 10^{-16}$ s $= 100$ attosec.

4.3.1 Classical, Anharmonic Oscillator Model of Electronic Nonlinearities

A simple model of electronic nonlinearities is the classical, anharmonic oscillator model presented in Section 1.4. According to this model, one assumes that the potential well binding the electron to the atomic nucleus deviates from the parabolic potential of the usual Lorentz model. We approximate the actual potential well as

$$U(\mathrm{r}) = \tfrac{1}{2}m\omega_0^2|\mathrm{r}|^2 - \tfrac{1}{4}mb|\mathbf{r}|^4, \tag{4.3.1}$$

where b is a phenomenological nonlinear constant whose value is of the order of ω_0^2/d^2, where d is a typical atomic dimension. By solving the equation of motion for an electron in such a potential well, we obtain expression (1.4.52) for the third-order susceptibility. When applied to the case of the nonlinear refractive index, this expression becomes

$$\chi^{(3)}_{ijkl}(\omega = \omega + \omega - \omega) = \frac{Nbe^4[\delta_{ij}\delta_{kl} + \delta_{ik}\delta_{jl} + \delta_{il}\delta_{jk}]}{3\epsilon_0 m^3 D(\omega)^3 D(-\omega)}, \tag{4.3.2}$$

where $D(\omega) = \omega_0^2 - \omega^2 - 2i\omega\gamma$. In the notation of Maker and Terhune (Eq. (4.2.10)), this result implies that

$$A = B = \frac{2Nbe^4}{\epsilon_0 m^3 D(\omega)^3 D(-\omega)}. \tag{4.3.3}$$

Hence, according to the classical, anharmonic oscillator model of electronic nonlinearities, A is equal to B for any value of the optical field frequency (whether resonant or nonresonant). For the case of far-off-resonant excitation (i.e., $\omega \ll \omega_0$), we can replace $D(\omega)$ by ω_0^2 in Eq. (4.3.2). If in addition we set b equal to ω_0^2/d^2, we find that

$$\chi^{(3)} \simeq \frac{Ne^4}{\epsilon_0 m^3 \omega_0^6 d^2}. \tag{4.3.4}$$

For the typical values $N = 4 \times 10^{22}$ cm^{-3}, $d = 3 \times 10^{-10}$ m, and $\omega_0 = 7 \times 10^{15}$ rad/s, we find that $\chi^{(3)} \simeq 3 \times 10^{-22}$ m^2/V^2.

4.3.2 Quantum-Mechanical Model of Nonresonant Electronic Nonlinearities

Let us now see how to calculate the third-order susceptibility describing the nonlinear refractive index using the laws of quantum mechanics. Since we are interested primarily in the case of nonresonant excitation, we make use of the expression for the nonlinear susceptibility in the

form given by Eq. (3.2.31)—that is,

$$\chi^{(3)}_{kjih}(\omega_\sigma, \omega_r, \omega_q, \omega_p) = \frac{N}{\epsilon_0 \hbar^3} \mathcal{P}_F \sum_{lmn} \left[\frac{\mu^k_{gn} \mu^j_{nm} \mu^i_{ml} \mu^h_{lg}}{(\omega_{ng} - \omega_\sigma)(\omega_{mg} - \omega_q - \omega_p)(\omega_{lg} - \omega_p)} \right], \tag{4.3.5}$$

where $\omega_\sigma = \omega_r + \omega_q + \omega_p$. We want to apply this expression to the case of the nonlinear refractive index, with the frequencies arranged as $\chi^{(3)}_{kjih}(\omega, \omega, \omega, -\omega) = \chi^{(3)}_{kjih}(\omega = \omega + \omega - \omega)$. One sees that Eq. (4.3.5) appears to have divergent contributions for this choice of frequencies, because the factor $\omega_{mg} - \omega_q - \omega_p$ in the denominator vanishes when the dummy index m is equal to g and when $\omega_p = -\omega_q = \pm\omega$. However, in fact this divergence exists in appearance only (Hanna et al., 1979; Orr and Ward, 1971); one can readily rearrange Eq. (4.3.5) into a form where no divergence appears. We first rewrite Eq. (4.3.5) as

$$\chi^{(3)}_{kjih}(\omega_\sigma, \omega_r, \omega_q, \omega_p) = \frac{N}{\epsilon_0 \hbar^3} \mathcal{P}_F \left[\sum_{lmn}{}' \frac{\mu^k_{gn} \mu^j_{nm} \mu^i_{ml} \mu^h_{lg}}{(\omega_{ng} - \omega_\sigma)(\omega_{mg} - \omega_q - \omega_p)(\omega_{lg} - \omega_p)} - \sum_{ln} \frac{\mu^k_{gn} \mu^j_{ng} \mu^i_{gl} \mu^h_{lg}}{(\omega_{ng} - \omega_\sigma)(\omega_q + \omega_p)(\omega_{lg} - \omega_p)} \right]. \tag{4.3.6}$$

Here the prime on the first summation indicates that the terms corresponding to $m = g$ are to be omitted from the summation over m; these terms are displayed explicitly in the second summation. The second summation, which appears to be divergent for $\omega_q = -\omega_p$, is now rearranged. We make use of the identity

$$\frac{1}{XY} = \frac{1}{(X+Y)Y} + \frac{1}{(X+Y)X}, \tag{4.3.7}$$

with $X = \omega_q + \omega_p$ and $Y = \omega_{lg} - \omega_p$, to express Eq. (4.3.6) as

$$\chi^{(3)}_{kjih}(\omega_\sigma, \omega_r, \omega_q, \omega_p) = \frac{N}{\epsilon_0 \hbar^3} \mathcal{P}_F \left[\sum_{lmn}{}' \frac{\mu^k_{gn} \mu^j_{nm} \mu^i_{ml} \mu^h_{lg}}{(\omega_{ng} - \omega_\sigma)(\omega_{mg} - \omega_q - \omega_p)(\omega_{lg} - \omega_p)} - \sum_{ln} \frac{\mu^k_{gn} \mu^j_{ng} \mu^i_{gl} \mu^h_{lg}}{(\omega_{ng} - \omega_\sigma)(\omega_{lg} + \omega_q)(\omega_{lg} - \omega_p)} \right] \tag{4.3.8}$$

in addition to the contribution

$$\mathcal{P}_F \sum_{ln} \frac{\mu_{gn}^k \mu_{ng}^j \mu_{gl}^i \mu_{lg}^h}{(\omega_{ng} - \omega_\sigma)(\omega_{lg} + \omega_q)(\omega_q + \omega_p)}. \tag{4.3.9}$$

However, this additional contribution vanishes, because for every term of the form

$$\frac{\mu_{gn}^k \mu_{ng}^j \mu_{gl}^i \mu_{lg}^h}{(\omega_{ng} - \omega_\sigma)(\omega_{lg} + \omega_q)(\omega_q + \omega_p)} \tag{4.3.10a}$$

that appears in Eq. (4.3.9), there is another term with the dummy summation indices n and l interchanged, with the pair $(-\omega_\sigma, k)$ interchanged with (ω_q, i), and with the pair (ω_p, h) interchanged with (ω_r, j); this term is of the form

$$\frac{\mu_{gl}^i \mu_{lg}^h \mu_{gn}^k \mu_{ng}^j}{(\omega_{lg} + \omega_q)(\omega_{ng} - \omega_\sigma)(\omega_r - \omega_\sigma)}. \tag{4.3.10b}$$

Since $\omega_\sigma = \omega_p + \omega_q + \omega_r$, it follows that $(\omega_q + \omega_p) = -(\omega_r - \omega_\sigma)$, and hence the expression (4.3.10a) and (4.3.10b) are equal in magnitude but opposite in sign. The expression (4.3.8) for the nonlinear susceptibility is thus equivalent to Eq. (4.3.5) but is more useful for our present purpose because no apparent divergences are present.

We now specialize Eq. (4.3.8) to the case of the nonlinear refractive index with the choice of frequencies given by $\chi_{kjih}^{(3)}(\omega, \omega, \omega, -\omega)$. When we expand the permutation operator $\mathcal{P}_F$, we find that each displayed term in Eq. (4.3.8) actually represents 24 terms. The resonance nature of each such term can be analyzed by means of diagrams of the sort shown in Fig. 3.2.3.* Rather than considering all 48 terms of the expanded version of Eq. (4.3.8), let us consider only the nearly resonant terms, which would be expected to make the largest contributions to $\chi^{(3)}$. One finds, after detailed analysis of Eq. (4.3.8), that the resonant contribution to the nonlinear susceptibility is given by

$$\begin{aligned}
&\chi_{kjih}^{(3)}(\omega, \omega, \omega, -\omega) = \chi_{kjih}^{(3)}(\omega = \omega + \omega - \omega) = \frac{N}{6\epsilon_0 \hbar^3} \\
&\times \left({\sum_{lmn}}' \frac{\mu_{gn}^k \mu_{nm}^h \mu_{ml}^i \mu_{lg}^j + \mu_{gn}^k \mu_{nm}^h \mu_{ml}^j \mu_{lg}^i + \mu_{gn}^h \mu_{nm}^k \mu_{ml}^i \mu_{lg}^j + \mu_{gn}^h \mu_{nm}^k \mu_{ml}^j \mu_{lg}^i}{(\omega_{ng} - \omega)(\omega_{mg} - 2\omega)(\omega_{lg} - \omega)} \right. \\
&\left. - \sum_{ln} \frac{\mu_{gn}^k \mu_{ng}^j \mu_{gl}^h \mu_{lg}^i + \mu_{gn}^k \mu_{ng}^i \mu_{gl}^h \mu_{lg}^j + \mu_{gn}^h \mu_{ng}^i \mu_{gl}^k \mu_{lg}^j + \mu_{gn}^h \mu_{ng}^j \mu_{gl}^k \mu_{lg}^i}{(\omega_{ng} - \omega)(\omega_{lg} - \omega)(\omega_{lg} - \omega)} \right).
\end{aligned} \tag{4.3.11}$$

* Note, however, that Fig. 3.2.3 as drawn presupposes that the three input frequencies are all positive, whereas for the case of the nonlinear refractive index two of the input frequencies are positive and one is negative.

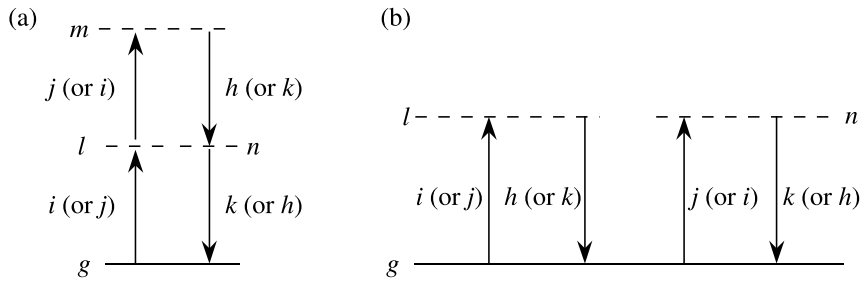

FIGURE 4.3.1: Resonance nature of the first (a) and second (b) summations of Eq. (4.3.11).

Here the first summation represents two-photon-resonant processes and the second summation represents one-photon-resonant processes, in the sense illustrated in Fig. 4.3.1.

We can use Eq. (4.3.11) to obtain explicit expressions for the resonant contributions to the nonvanishing elements of the nonlinear susceptibility tensor for an isotropic medium. We find, for example, that $\chi_{1111}(\omega = \omega + \omega - \omega)$ is given by

$$\chi_{1111} = \frac{2N}{3\epsilon_0\hbar^3}\sum_{lmn}{}' \frac{\mu_{gn}^x \mu_{nm}^x \mu_{ml}^x \mu_{lg}^x}{(\omega_{ng}-\omega)(\omega_{mg}-2\omega)(\omega_{lg}-\omega)} - \frac{2N}{3\epsilon_0\hbar^3}\sum_{ln} \frac{\mu_{gn}^x \mu_{ng}^x \mu_{gl}^x \mu_{lg}^x}{(\omega_{ng}-\omega)(\omega_{lg}-\omega)(\omega_{lg}-\omega)}. \tag{4.3.12}$$

Note that both one- and two-photon-resonant terms contribute to this expression. When ω is smaller than any resonant frequency of the material system, the two-photon contribution (the first term) tends to be positive. This contribution is positive because, in the presence of an applied optical field, there is some nonzero probability that the atom will reside in an excited state (state l or n as Fig. 4.3.1(a) is drawn). Since the (linear) polarizability of an atom in an excited state tends to be larger than that of an atom in the ground state, the effective polarizability of an atom is increased by the presence of an intense optical field; consequently this contribution to $\chi^{(3)}$ is positive. On the other hand, the one-photon contribution to χ_{1111} (the second term of Eq. (4.3.12)) is always negative when ω is smaller than any resonance frequency of the material system, because the product of matrix elements that appears in the numerator of this term is positive definite. We can understand this result from the point of view that the origin of one-photon-resonant contributions to the nonlinear susceptibility is saturation of the atomic response, which in the present case corresponds to a decrease of the positive linear susceptibility. We can also understand this result as a consequence of the ac Stark effect, which (as we shall see in Section 6.5) leads to an intensity-dependent increase in the separation of the lower and upper levels and consequently to a diminished optical response, as illustrated in Fig. 4.3.2.

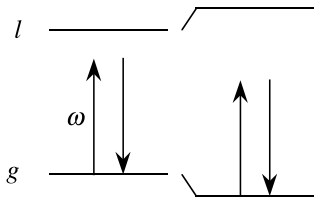

FIGURE 4.3.2: For $\omega < \omega_{lg}$ the ac Stark effect leads to an increase in the energy separation of the ground and excited states.

In a similar fashion, we find that the resonant contribution to χ_{1221} (or to $\frac{1}{6}B$ in the notation of Maker and Terhune) is given by

$$\chi_{1221} = \frac{2}{3}\frac{N}{\epsilon_0\hbar^3}\sum_{lmn}{}' \frac{\mu_{gn}^x \mu_{nm}^x \mu_{ml}^y \mu_{lg}^y}{(\omega_{ng}-\omega)(\omega_{mg}-2\omega)(\omega_{lg}-\omega)}. \tag{4.3.13}$$

The one-photon-resonant terms do not contribute to χ_{1221}, since these terms involve the summation of the product of two matrix elements of the sort $\mu_{gl}^x \mu_{lg}^y$, and this contribution always vanishes.*

We also find that the resonant contribution to χ_{1122} (or to $\frac{1}{6}A$) is given by

$$\begin{aligned}\chi_{1122} = {} & \frac{N}{3\epsilon_0\hbar^3}\sum_{lmn}{}' \frac{(\mu_{gn}^x \mu_{nm}^y \mu_{ml}^y \mu_{lg}^x + \mu_{gn}^x \mu_{nm}^y \mu_{ml}^x \mu_{lg}^y)}{(\omega_{ng}-\omega)(\omega_{mg}-2\omega)(\omega_{lg}-\omega)} \\ & - \frac{N}{3\epsilon_0\hbar^3}\sum_{ln}\frac{\mu_{gn}^x \mu_{ng}^x \mu_{gl}^y \mu_{lg}^y}{(\omega_{ng}-\omega)(\omega_{mg}-\omega)(\omega_{lg}-\omega)}.\end{aligned} \tag{4.3.14}$$

4.3.3 $\chi^{(3)}$ in the Low-Frequency Limit

In practice, one is often interested in determining the value of the third-order susceptibility under highly nonresonant conditions—that is, for the case in which the optical frequency is very much smaller than any resonance frequency of the atomic system. An example would be the nonlinear response of an insulating solid to visible radiation. In such cases, each of the terms in the expansion of the permutation operator in Eq. (4.3.8) makes a comparable contribution to the nonlinear susceptibility, and no simplification such as those leading to Eqs. (4.3.11) through (4.3.14) is possible. It is an experimental fact that in the low-frequency limit both χ_{1122} and χ_{1221} (and consequently $\chi_{1111} = 2\chi_{1122} + \chi_{1221}$) are positive in sign for the vast majority of

* To see that this contribution vanishes, choose x to be the quantization axis. Then if μ_{gl}^x is nonzero, μ_{gl}^y must vanish, and vice versa.

TABLE 4.3.1: Nonlinear optical coefficient for materials showing electronic nonlinearities[a].

Material	n_0	χ_{1111} (m^2/V^2)	n_2 (m^2/W)
Diamond	2.42	21×10^{-22}	10×10^{-20}
Yttrium aluminum garnet	1.83	8.4×10^{-22}	8.4×10^{-20}
Sapphire	1.8	4.2×10^{-22}	3.7×10^{-20}
Borosilicate crown glass	1.5	3.5×10^{-22}	4.4×10^{-20}
Fused silica	1.47	2.8×10^{-22}	3.67×10^{-20}
CaF_2	1.43	2.24×10^{-22}	3.1×10^{-20}
LiF	1.4	1.4×10^{-22}	2.0×10^{-20}

[a] Values are obtained from optical frequency mixing experiments and hence do not include electrostrictive contributions, since electrostriction is a slow process that cannot respond at optical frequencies. The value of $\bar{n}_2$ is calculated as $\bar{n}_2 = 3\pi\chi_{1111}/n_0$. (Adapted from Hellwarth (1977), Tables 7.1 and 9.1.)

optical materials. Also, the Kleinman symmetry condition becomes relevant under conditions of low-frequency excitation, which implies that χ_{1122} is equal to χ_{1221}, or that B is equal to A in the notation of Maker and Terhune.

We can use the results of the quantum-mechanical model to make an order-of-magnitude prediction of the value of the nonresonant third-order susceptibility. If we assume that the optical frequency ω is much smaller than all atomic resonance frequencies, we find from Eq. (4.3.5) that the nonresonant value of the nonlinear optical susceptibility is given by

$$\chi^{(3)} \simeq \frac{8N\mu^4}{\epsilon_0 \hbar^3 \omega_0^3}, \tag{4.3.15}$$

where μ is a typical value of the dipole matrix element and ω_0 is a typical value of the atomic resonance frequency. It should be noted that while the predictions of the classical model (Eq. (4.3.4)) and the quantum-mechanical model (Eq. (4.3.15)) show different functional dependences on the displayed variables, the two expressions are in fact equal if we identify d with the Bohr radius $a_0 = 4\pi\epsilon_0\hbar^2/me^2$, μ with the atomic unit of electric dipole moment $-ea_0$, and ω_0 with the Rydberg constant in angular frequency units, $\omega_0 = me^4/32\pi^2\epsilon_0^2\hbar^3$. Hence, the quantum-mechanical model also predicts that the third-order susceptibility is of the order of magnitude of 3×10^{-22} m^2/V^2. The measured values of $\chi^{(3)}$ and n_2 for several materials that display nonresonant electronic nonlinearities are given in Table 4.3.1.

4.4 Nonlinearities Due to Molecular Orientation

Liquids that are composed of anisotropic molecules (i.e., molecules having an anisotropic polarizability tensor) typically possess a large value of n_2. The origin of this nonlinearity is the tendency of molecules to become aligned in the electric field of an applied optical wave. The

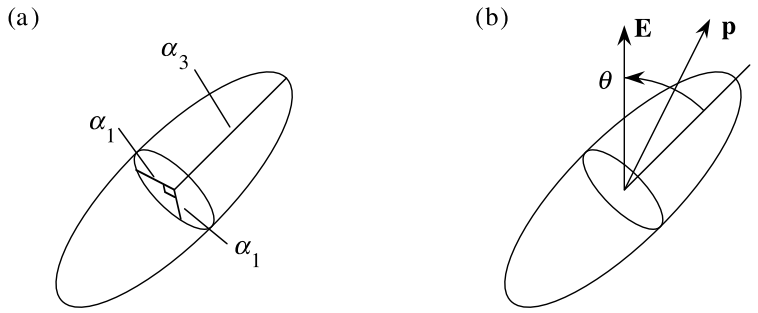

FIGURE 4.4.1: (a) A prolate spheroidal molecule, such as carbon disulfide. (b) The dipole moment **p** induced by an electric field **E**.

optical wave then experiences a modified value of the refractive index because the average polarizability per molecule has been changed by the molecular alignment.

Consider, for example, the case of carbon disulfide (CS_2), which is illustrated in part (a) of Fig. 4.4.1. Carbon disulfide is a cigar-shaped molecule (i.e., a prolate spheroid), and consequently the polarizability α_3 experienced by an optical field that is parallel to the symmetry axis is larger than the polarizability α_1 experienced by a field that is perpendicular to its symmetry axis—that is,

$$\alpha_3 > \alpha_1. \tag{4.4.1}$$

Consider now what happens when such a molecule is subjected to a static electric field, as shown in part (b) of the figure. Since α_3 is larger than α_1, the component of the induced dipole moment along the molecular axis will be disproportionately long. The induced dipole moment **p** thus will not be parallel to **E** but will be offset from it in the direction of the symmetry axis. A torque

$$\boldsymbol{\tau} = \mathbf{p} \times \mathbf{E} \tag{4.4.2}$$

will thus be exerted on the molecule. This torque is directed in such a manner as to twist the molecule into alignment with the applied electric field.

The tendency of the molecule to become aligned in the applied electric field is counteracted by thermal agitation, which tends to randomize the molecular orientation. The mean degree of molecular orientation is quantified through use of the Boltzmann factor. To determine the Boltzmann factor, we first calculate the potential energy of the molecule in the applied electric field. If the applied field is changed by an amount $d\mathbf{E}$, the orientational potential energy is changed by the amount

$$dU = -\mathbf{p} \cdot d\mathbf{E} = -p_3\, dE_3 - p_1\, dE_1, \tag{4.4.3}$$

where we have decomposed **E** into its components along the molecular axis (E_3) and perpendicular to the molecular axis (E_1). Since

$$p_3 = \alpha_3 E_3 \tag{4.4.4}$$

and

$$p_1 = \alpha_1 E_1, \tag{4.4.5}$$

we find that

$$dU = -\alpha_3 E_3\, dE_3 - \alpha_1 E_1\, dE_1, \tag{4.4.6}$$

which can be integrated to give

$$U = -\tfrac{1}{2}\left(\alpha_3 E_3^2 + \alpha_1 E_1^2\right). \tag{4.4.7}$$

If we now introduce the angle θ between **E** and the molecular axis (see Fig. 4.4.1(b)), we find that the orientational potential energy is given by

$$\begin{aligned} U &= -\tfrac{1}{2}\left[\alpha_3 E^2 \cos^2\theta + \alpha_1 E^2 \sin^2\theta\right] \\ &= -\tfrac{1}{2}\alpha_1 E^2 - \tfrac{1}{2}(\alpha_3 - \alpha_1) E^2 \cos^2\theta. \end{aligned} \tag{4.4.8}$$

Since $\alpha_3 - \alpha_1$ has been assumed to be positive, this result shows that the potential energy is lower when the molecular axis is parallel to **E** than when it is perpendicular to **E**, as illustrated in Fig. 4.4.2.

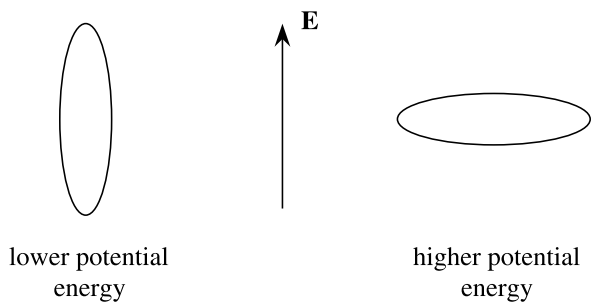

FIGURE 4.4.2: Alignment energy of a molecule.

Our discussion thus far has assumed that the applied field is static. We now allow the field to vary in time at an optical frequency. For simplicity we assume that the light is linearly polarized; the general case of elliptical polarization is treated at the end of the present section. We thus replace **E** in Eq. (4.4.9) by the time-varying scalar quantity $\tilde{E}(t)$. The square of $\tilde{E}$ will contain frequency components near zero frequency and components at approximately twice the optical

frequency ω. Since orientational relaxation times for molecules are typically of the order of a few picoseconds, the molecular orientation can respond to the frequency components near zero frequency but not to those near 2ω. We can thus formally replace E^2 in Eq. (4.4.9) by $\overline{\tilde{E}^2}$, where the bar denotes a time average over many cycles of the optical field.

We now calculate the intensity-dependent refractive index for such a medium. For simplicity, we first ignore local-field corrections, in which case the refractive index is given by

$$n^2 = 1 + \chi = 1 + N\langle\alpha\rangle, \tag{4.4.9}$$

where N is the number density of molecules and where $\langle\alpha\rangle$ denotes the expectation value of the molecular polarizability experienced by the incident radiation. To obtain an expression for $\langle\alpha\rangle$, we note that the mean orientational potential energy is given by $\langle U\rangle = -\frac{1}{2}|E|^2\langle\alpha\rangle$, which by comparison with the average of Eq. (4.4.8) shows that

$$\langle\alpha\rangle = \alpha_3\langle\cos^2\theta\rangle + \alpha_1\langle\sin^2\theta\rangle = \alpha_1 + (\alpha_3 - \alpha_1)\langle\cos^2\theta\rangle. \tag{4.4.10}$$

Here $\langle\cos^2\theta\rangle$ denotes the expectation value of $\cos^2\theta$ in thermal equilibrium and is given in terms of the Boltzmann distribution as

$$\langle\cos^2\theta\rangle = \frac{\int d\Omega \cos^2\theta \exp[-U(\theta)/kT]}{\int d\Omega \exp[-U(\theta)/kT]}, \tag{4.4.11}$$

where $\int d\Omega$ denotes an integration over all solid angles. For convenience, we introduce the intensity parameter

$$J = \tfrac{1}{2}(\alpha_3 - \alpha_1)\overline{\tilde{E}^2}/kT, \tag{4.4.12}$$

and let $d\Omega = 2\pi \sin\theta d\theta$. We then find that $\langle\cos^2\theta\rangle$ is given by

$$\langle\cos^2\theta\rangle = \frac{\int_0^\pi \cos^2\theta \exp(J\cos^2\theta)\sin\theta\, d\theta}{\int_0^\pi \exp(J\cos^2\theta)\sin\theta\, d\theta}. \tag{4.4.13}$$

Eqs. (4.4.9) through (4.4.13) can be used to determine the refractive index experienced by fields of arbitrary intensity $\overline{\tilde{E}^2}$.

Let us first calculate the refractive index experienced by a weak optical field, by taking the limit $J \to 0$. For this case we find that the average of $\cos^2\theta$ is given by

$$\langle\cos^2\theta\rangle_0 = \frac{\int_0^\pi \cos^2\theta \sin\theta\, d\theta}{\int_0^\pi \sin\theta\, d\theta} = \tfrac{1}{3} \tag{4.4.14}$$

and that according to Eq. (4.4.10), the mean polarizability is given by

$$\langle\alpha\rangle_0 = \tfrac{1}{3}\alpha_3 + \tfrac{2}{3}\alpha_1. \tag{4.4.15}$$

Using Eq. (4.4.9), we find that the refractive index is given by

$$n_0^2 = 1 + N\left(\tfrac{1}{3}\alpha_3 + \tfrac{2}{3}\alpha_1\right). \tag{4.4.16}$$

Note that this result makes good physical sense: in the absence of processes that tend to align the molecules, the mean polarizability is equal to one-third of that associated with the direction of the symmetry axis of the molecule plus two-thirds of that associated with directions perpendicular to this axis.

For the general case in which an intense optical field is applied, we find from Eqs. (4.4.9) and (4.4.10) that the refractive index is given by

$$n^2 = 1 + N\left[\alpha_1 + (\alpha_3 - \alpha_1)\left\langle\cos^2\theta\right\rangle\right], \tag{4.4.17}$$

and thus by comparison with Eq. (4.4.16) that the square of the refractive index changes by the amount

$$\begin{aligned} n^2 - n_0^2 &= N\left[\tfrac{1}{3}\alpha_1 + (\alpha_3 - \alpha_1)\left\langle\cos^2\theta\right\rangle - \tfrac{1}{3}\alpha_3\right] \\ &= N(\alpha_3 - \alpha_1)\left(\left\langle\cos^2\theta\right\rangle - \tfrac{1}{3}\right). \end{aligned} \tag{4.4.18}$$

Since $n^2 - n_0^2$ is usually very much smaller than n_0^2, we can express the left-hand side of this equation as

$$n^2 - n_0^2 = (n - n_0)(n + n_0) \simeq 2n_0(n - n_0)$$

and thus find that the refractive index can be expressed as

$$n = n_0 + \delta n, \tag{4.4.19}$$

where the nonlinear change in refractive index is given by

$$\delta n \equiv n - n_0 = \frac{N}{2n_0}(\alpha_3 - \alpha_1)\left(\left\langle\cos^2\theta\right\rangle - \tfrac{1}{3}\right). \tag{4.4.20}$$

The quantity $\langle\cos^2\theta\rangle$, given by Eq. (4.4.13), can be calculated in terms of a tabulated function (the Dawson integral). Fig. 4.4.3 shows a plot of $\langle\cos^2\theta\rangle - \frac{1}{3}$ as a function of the intensity parameter $J = \frac{1}{2}(\alpha_3 - \alpha_1)\overline{\tilde{E}^2}/kT$.

In order to obtain an explicit formula for the change in refractive index, we expand the exponentials appearing in Eq. (4.4.13) and integrate the resulting expression term by term. We find that

$$\left\langle\cos^2\theta\right\rangle = \frac{1}{3} + \frac{4J}{45} + \frac{8J^2}{945} + \cdots. \tag{4.4.21}$$

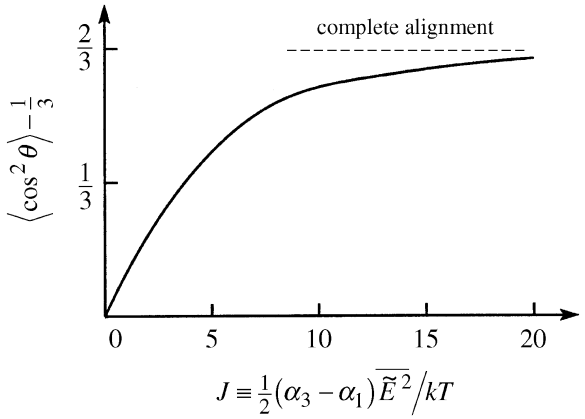

FIGURE 4.4.3: Variation of the quantity $(\langle \cos^2\theta \rangle - \frac{1}{3})$, which is proportional to the nonlinear change in refractive index δn, with the intensity parameter J. Note that for $J \lesssim 5$, δn increases nearly linearly with J.

Dropping all terms but the first two, we find from (4.4.20) that the change in the refractive index due to the nonlinear interaction is given by

$$\delta n = \frac{N}{2n_0}(\alpha_3 - \alpha_1)\frac{4J}{45} = \frac{N}{45n_0}(\alpha_3 - \alpha_1)^2\frac{\overline{\tilde{E}^2}}{kT}. \tag{4.4.22}$$

We can express this result as

$$\delta n = \bar{n}_2\overline{\tilde{E}^2}, \tag{4.4.23}$$

where the second-order nonlinear refractive index is given by

$$\bar{n}_2 = \frac{N}{45n_0}\frac{(\alpha_3 - \alpha_1)^2}{kT}. \tag{4.4.24a}$$

Equivalently, we find through use of Eq. (4.1.18) that

$$n_2 = \frac{N}{45n_0n_0'\epsilon_0 c}\frac{(\alpha_3 - \alpha_1)^2}{kT}, \tag{4.4.24b}$$

using the convention that $n = n_0 + n_2 I$ and where n_0' is the real part of n_0. Note that n_2 is positive both for the case $\alpha_3 > \alpha_1$ (the case that we have been considering explicitly) and for the opposite case where $\alpha_3 < \alpha_1$. The reason for this behavior is that the torque experienced by the molecule is always directed in a manner that tends to align the molecule so that the light sees a *larger* value of the polarizability.

A more accurate prediction of the nonlinear refractive index is obtained by including the effects of local-field corrections. We begin with the Lorentz–Lorenz law (see also Eq. (3.9.8a)),

$$\frac{n^2-1}{n^2+2}=\frac{1}{3}N\langle\alpha\rangle, \tag{4.4.25}$$

instead of the approximate relationship (4.4.9). By repeating the derivation leading to Eq. (4.4.24a) with Eq. (4.4.9) replaced by Eq. (4.4.25) and with the time average of $\tilde{E}^2$ replaced by that of the Lorentz local field (see the discussion of Section 3.9), we find that the second-order nonlinear refractive index is given by

$$\bar{n}_2=\frac{N}{45n_0n_0'\epsilon_0c}\left(\frac{n_0^2+2}{3}\right)^4\frac{(\alpha_3-\alpha_1)^2}{kT}. \tag{4.4.26}$$

Note that this result is consistent with the general prescription given in Section 3.9, which states that local-field effects can be included by multiplying the results obtained in the absence of local field corrections (that is, Eq. (4.4.24b)) by the local-field correction factor $\mathcal{L}^{(3)}=[(n_0^2+2)/3]^4$ of Eq. (3.9.25).

Finally, we quote some numerical values relevant to the material carbon disulfide. The maximum possible value of δn is 0.58 and would correspond to a complete alignment of the molecules. The value $J=1$ corresponds to a field strength of $E\simeq 3\times 10^9$ V/m. Through use of Eqs. (4.4.12) and (4.4.24b) and the value $n_0=1.63$, we find that $n_2=3\times 10^{-22}$ m^2/W.

4.4.1 Tensor Properties of $\chi^{(3)}$ for the Molecular Orientation Effect

Let us now consider the nonlinear response of a collection of anisotropic molecules to light of arbitrary polarization. Close et al. (1966) have shown that the mean polarizability in thermal equilibrium for a molecule whose three principal polarizabilities a, b, and c are distinct can be represented as

$$\langle\alpha_{ij}\rangle=\alpha\delta_{ij}+\gamma_{ij}, \tag{4.4.27}$$

where the linear contribution to the mean polarizability is given by

$$\alpha=\tfrac{1}{3}(a+b+c), \tag{4.4.28}$$

and where the lowest-order nonlinear correction term is given by

$$\gamma_{ij}=C\sum_{kl}(3\delta_{ik}\delta_{jl}-\delta_{ij}\delta_{kl})\overline{\tilde{E}_k^{\mathrm{loc}}(t)\tilde{E}_l^{\mathrm{loc}}(t)}. \tag{4.4.29}$$

Here the constant C is given by

$$C = \frac{(a-b)^2 + (b-c)^2 + (a-c)^2}{90kT}, \tag{4.4.30}$$

and $\tilde{E}^{\text{loc}}$ denotes the Lorentz local field. In the appendix to this section, we derive the result given by Eqs. (4.4.27) through (4.4.30) for the special case of an axially symmetric molecule; the derivation for the general case is left as an exercise to the reader. Next, we use these results to determine the form of the third-order susceptibility tensor. We first ignore local-field corrections and replace $\tilde{E}_k^{\text{loc}}(t)$ by the microscopic electric field $\tilde{E}_k(t)$, which we represent as

$$\tilde{E}_k(t) = E_k e^{-i\omega t} + \text{c.c.} \tag{4.4.31}$$

The electric-field-dependent factor appearing in Eq. (4.4.29) thus becomes

$$\overline{\tilde{E}_k^{\text{loc}}(t)\tilde{E}_l^{\text{loc}}(t)} = E_k E_l^* + E_k^* E_l. \tag{4.4.32}$$

Since we are ignoring local-field corrections, we can assume that the polarization is given by

$$P_i = \epsilon_0 \sum_j N\langle\alpha_{ij}\rangle E_j \tag{4.4.33}$$

and thus that the third-order contribution to the polarization is given by

$$P_i^{(3)} = \epsilon_0 N \sum_j \gamma_{ij} E_j. \tag{4.4.34}$$

By introducing the form for γ_{ij} given by Eqs. (4.4.29) and (4.4.32) into this expression, we find that

$$P_i^{(3)} = \epsilon_0 NC \sum_{jkl} (3\delta_{ik}\delta_{jl} - \delta_{ij}\delta_{kl})(E_k E_l^* + E_k^* E_l) E_j,$$

which can be written entirely in vector form as

$$\begin{aligned} \mathbf{P}^{(3)} &= \epsilon_0 NC\big[3(\mathbf{E}\cdot\mathbf{E}^*)\mathbf{E} + 3(\mathbf{E}\cdot\mathbf{E})\mathbf{E}^* - (\mathbf{E}\cdot\mathbf{E}^*)\mathbf{E} - (\mathbf{E}\cdot\mathbf{E}^*)\mathbf{E}\big] \\ &= \epsilon_0 NC\big[(\mathbf{E}\cdot\mathbf{E}^*)\mathbf{E} + 3(\mathbf{E}\cdot\mathbf{E})\mathbf{E}^*\big]. \end{aligned} \tag{4.4.35}$$

This result can be rewritten using the notation of Maker and Terhune (see also Eq. (4.2.10)) as

$$\mathbf{P}^{(3)} = \epsilon_0 A(\mathbf{E}\cdot\mathbf{E}^*)\mathbf{E} + \tfrac{1}{2}\epsilon_0 B(\mathbf{E}\cdot\mathbf{E})\mathbf{E}^*, \tag{4.4.36}$$

where the coefficients A and B are given by $B = 6A = 6NC$, which through use of the expression (4.4.30) for C becomes

$$B = 6A = N\left[\frac{(a-b)^2 + (b-c)^2 + (a-c)^2}{15kT}\right]. \tag{4.4.37}$$

This result shows that for the molecular orientation effect the ratio B/A is equal to 6, a result quoted earlier without proof (in (4.2.13a)). As in Eq. (4.4.26), local-field corrections can be included in the present formalism by replacing Eq. (4.4.37) by

$$B = 6A = \left(\frac{n_0^2+2}{3}\right)^4 N\left[\frac{(a-b)^2+(b-c)^2+(a-c)^2}{15kT}\right]. \tag{4.4.38}$$

4.5 Thermal Nonlinear Optical Effects

Thermal processes can lead to large (and often unwanted) nonlinear optical effects. The origin of thermal nonlinear optical effects is that some fraction of the incident laser power is absorbed in passing through an optical material. The temperature of the illuminated portion of the material consequently increases, which leads to a change in the refractive index of the material. For gases, the refractive index invariably decreases with increasing temperature (at constant pressure), but for condensed matter the refractive index can either increase or decrease with changes in temperature, depending on details of the internal structure of the material. The time scale for changes in the temperature of the material can be quite long (of the order of seconds), and consequently thermal effects often lead to strongly time-dependent nonlinear optical phenomena.

Thermal effects can be described mathematically by assuming that the refractive index $\tilde{n}$ varies with temperature according to*

$$\tilde{n} = n_0 + \left(\frac{dn}{dT}\right)\tilde{T}_1, \tag{4.5.1}$$

where the quantity (dn/dT) describes the temperature dependence of the refractive index of a given material and where $\tilde{T}_1$ designates the laser-induced change in temperature. We assume that $\tilde{T}_1$ obeys the heat-transport equation

$$(\rho_0 C)\frac{\partial \tilde{T}_1}{\partial t} - \kappa\nabla^2\tilde{T}_1 = \alpha\tilde{I}(r). \tag{4.5.2}$$

Here $(\rho_0 C)$ denotes the heat capacity per unit volume, κ denotes the thermal conductivity, and α denotes the linear absorption coefficient of the material. We express the heat capacity in the form $(\rho_0 C)$ because most handbooks tabulate the material density ρ_0 and the heat capacity per unit mass C rather than their product $(\rho_0 C)$, which is the quantity of direct relevance in the present context. Representative values of dn/dT, $(\rho_0 C)$, and κ are shown in Table 4.5.1.

Eq. (4.5.2) can be solved as a boundary value problem for any specific physical circumstance, and hence the refractive index at any point in space can be found from Eq. (4.5.1). Note

* As elsewhere in this text, a tilde is used to designate an explicitly time-dependent quantity.

TABLE 4.5.1: Thermal properties of various optical materials.

Material	$(\rho_0 C)$ (J/cm^3)[a]	κ (W/m K)	dn/dT (K^{-1})[b]
Diamond	1.76	660	
Ethanol	1.91	0.168	
Fused silica	1.67	1.4	1.2×10^{-5}
Sodium chloride	1.95	6.4	-3.6×10^{-5}
Water (liquid)	4.2	0.56	
Air[c]	1.2×10^{-3}	26×10^{-3}	-1.0×10^{-6}

[a] $(\rho_0 C)$ is the heat capacity per unit volume and κ is the thermal conductivity. More extensive listings of these quantities can be found in the *CRC Handbook of Chemistry and Physics*, Section D, and in the *American Institute of Physics Handbook*, Section 4.
[b] dn/dT is the temperature coefficient of the refractive index. It can be either positive or negative, and for condensed matter typically lies in the range $\pm 3 \times 10^{-5}$ K^{-1}. See for instance the *American Institute of Physics Handbook*, Section 6b.
[c] C is measured at constant pressure. Values are quoted at STP. Under other conditions, the values of these quantities can be found by noting that to good approximation $(\rho_0 C)$ is proportional to the density, κ is independent of the density, and that for any ideal gas $dn/dT = -(n-1)/T$.

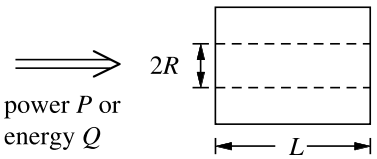

FIGURE 4.5.1: Geometry for the description of thermal nonlinear optical effects.

that thermal nonlinear optical effects are nonlocal, because the change in refractive index at some given point will in general depend on the laser intensity at other nearby points. For our present purposes, let us make some simple numerical estimates of the magnitude of the thermal contribution to the change in refractive index for the situation shown in Fig. 4.5.1. We assume that a circular laser beam of intensity I_0 and radius R (and consequently power $P = \pi R^2 I_0$) falls onto a slab of optical material of thickness L and absorption coefficient α.

Let us first estimate the response time τ associated with the change in temperature for this situation. We take τ to be some measure of the time taken for the temperature distribution to reach its new steady state after the laser field is suddenly switched on or is switched off. For definiteness we assume the latter situation. We then estimate τ by approximating $\partial \tilde{T}_1/\partial t$ in Eq. (4.5.2) by T_1/τ and by approximating $\nabla^2 \tilde{T}_1$ as T_1/R^2. Eq. (4.5.2) then becomes $(\rho_0 C) T_1/\tau \approx \kappa T_1/R^2$, from which it follows that

$$\tau \approx \frac{(\rho_0 C) R^2}{\kappa}. \tag{4.5.3}$$

We can estimate numerically the response time τ for condensed matter by adopting the typical values $(\rho_0 C) = 10^6$ J/m^3 K, $\kappa = 1$ W/m K, and $R = 1$ mm, and thus find that $\tau \approx 1$ s. Even for

a tightly collimated beam with $R = 10$ μm, we find that $\tau \approx 100$ μs. These response times are much longer than the pulse duration T produced by most pulsed lasers. One thus reaches the conclusion that, in the consideration of thermal effects, the power (or alternatively the intensity) is the relevant quantity for continuous-wave laser beams, but that the pulse energy $Q = PT$ (or alternatively the fluence, the energy per unit cross-sectional area) is the relevant quantity in the consideration of pulsed lasers.

4.5.1 Thermal Nonlinearities with Continuous-Wave Laser Beams

We have just seen that the analysis of thermal effects in nonlinear optics is different for continuous wave than for pulsed radiation. Let us consider first the case of continuous-wave radiation. Under steady-state conditions the equation of heat transport then reduces to

$$-\kappa \nabla^2 \tilde{T}_1 = \alpha \tilde{I}(r). \tag{4.5.4}$$

This equation can be solved explicitly for any assumed laser profile $\tilde{I}(r)$. For our present purposes it suffices to make an order-of-magnitude estimate of the maximum temperature rise $T_1^{(\max)}$ at the center of the laser beam. To do so, we replace $\nabla^2 \tilde{T}_1$ by $-T_1^{(\max)}/R^2$, and thereby find that

$$T_1^{(\max)} = \frac{\alpha I^{(\max)} R^2}{\kappa}, \tag{4.5.5}$$

where $I^{(\max)}$ is the laser intensity at the center of the laser beam. Then from Eq. (4.5.1) we estimate the maximum change in refractive index as

$$\Delta n = \left(\frac{dn}{dT}\right) \frac{\alpha I^{(\max)} R^2}{\kappa}. \tag{4.5.6}$$

We can express this change in terms of an effective nonlinear refractive index coefficient $n_2^{(\text{th})}$ defined through $\Delta n = n_2^{(\text{th})} I^{(\max)}$ to obtain

$$n_2^{(\text{th})} = \left(\frac{dn}{dT}\right) \frac{\alpha R^2}{\kappa}. \tag{4.5.7}$$

Note that this quantity is geometry-dependent (through the R^2 factor) and hence is not an intrinsic property of an optical material. Nonetheless, it provides a useful way of quantifying the magnitude of thermal nonlinear optical effects. If we estimate its size through use of the values $(dn/dT) = 10^{-5}$ K^{-1}, $\alpha = 1$ cm^{-1}, $R = 1$ mm, and $\kappa = 1$ W/m K, we find that $n_2^{(\text{th})} = 10^{-5}$ cm^2/W. By way of comparison, recall that for fused silica $n_2 = 3 \times 10^{-16}$ cm^2/W. Even for a much smaller beam size ($R = 10$ μm) and a much smaller absorption coefficient ($\alpha = 0.01$ cm^{-1}), we still obtain a relatively large thermal nonlinear coefficient of

$n_2^{(\mathrm{th})} = 10^{-11}$ cm^2/W. The conclusion to be drawn from these numbers is clear: thermal effects are usually the dominant nonlinear optical mechanism for continuous-wave laser beams. Analyses of thermal effects in nonlinear optics have been presented by Bespalov et al. (1989), Hoffman (1986), Martin and Hellwarth (1979), and Tochio et al. (1981). Recent experimental investigations of thermal nonlinear optical effects in gases have been reported by Bentley et al. (2000).

4.5.2 Thermal Nonlinearities with Pulsed Laser Beams

As mentioned earlier, for most pulsed lasers the induced change in refractive index is proportional to the pulse energy $Q = \int \tilde{P}(t)\,dt$ rather than to the instantaneous power $\tilde{P}(t)$ (or alternatively it is proportional to the pulse fluence $F = \int \tilde{I}(t)\,dt$ rather than to the pulse intensity $\tilde{I}(t)$). For this reason, it is not possible to describe the change in refractive index in terms of a quantity such as $n_2^{(\mathrm{th})}$. Rather, $\Delta\tilde{n}$ increases (or decreases) monotonically during the time extent of the laser pulse. Nonetheless one can develop simple criteria for determining the conditions under which thermal nonlinear optical effects are important. In particular, let us consider the conditions under which the thermal change in refractive index

$$\Delta n^{(\mathrm{th})} = \left(\frac{dn}{dT}\right) T_1^{(\max)} \tag{4.5.8}$$

will be greater than or equal to the change resulting from the electronic response

$$\Delta n^{(\mathrm{el})} = n_2^{(\mathrm{el})} I. \tag{4.5.9}$$

We estimate the maximum change in temperature $T_1^{(\max)}$ induced by the laser beam as follows: For a short laser pulse (pulse duration t_p much shorter than the thermal response time τ of Eq. (4.5.3)), the heat transport equation (4.5.2) reduces to

$$(\rho_0 C)\frac{\partial \tilde{T}_1}{\partial t} = \alpha \tilde{I}(r); \tag{4.5.10}$$

we have dropped the term $-\kappa\nabla^2\tilde{T}_1$ because in a time $t_p \ll \tau$ at most a negligible fraction of the absorbed energy can diffuse out of the interaction region. By approximating $\partial\tilde{T}_1/\partial t$ as $T_1^{(\max)}/t_p$, we find that

$$T_1^{(\max)} = \frac{\alpha I^{(\max)} t_p}{(\rho_0 C)}. \tag{4.5.11}$$

By combining Eqs. (4.5.8) through (4.5.11), we find that the thermal contribution to the change in refractive index will exceed the electronic contribution if the laser pulse duration satisfies the

inequality

$$t_p \geq \frac{n_2^{(\mathrm{el})}(\rho_0 C)}{(dn/dT)\alpha}. \tag{4.5.12}$$

If we evaluate this expression assuming the typical values $n_2^{(\mathrm{el})} = 3 \times 10^{-16}$ cm^2/W, $(\rho_0 C) = 1 \times 10^6$ J/m^3 K, $(dn/dT) = 1 \times 10^{-5}$ K^{-1}, $\alpha = 1$ cm^{-1}, we find that the condition for the importance of thermal effects becomes

$$t_p \geq 30 \text{ psec}. \tag{4.5.13}$$

We thus see that thermal effects are likely to make a contribution to the nonlinear optical response for all but the shortest ($t_p \ll 30$ psec) laser pulses.

4.6 Semiconductor Nonlinearities

Semiconductor materials play an important role in nonlinear optics both because they produce large nonlinear optical responses and because these materials lend themselves to the construction of integrated devices in which electronic, semiconductor laser, and nonlinear optical components are all fabricated on a single semiconductor substrate.

A key feature of semiconductor materials is that their allowed electronic energy states take the form of broad bands separated by forbidden regions. The filled or nearly filled bands are known as valence bands and the empty or partially empty bands are known as conduction bands. The energy separation between the highest valence band and the lowest conduction band is known as the band-gap energy E_g. These concepts are illustrated in Fig. 4.6.1(a). A crucial distinction associated with the nonlinear optical properties of a semiconductor material is whether the photon energy $\hbar\omega$ of the laser field is greater than or smaller than the band-gap energy. For $\hbar\omega > E_g$, as illustrated in part (b) of the figure, the nonlinear response results from the transfer of electrons to the conduction band, leading to a modification of the optical properties of the material. For the opposite case $\hbar\omega < E_g$ the nonlinear response is essentially instantaneous and occurs as the result of parametric processes involving virtual levels. We treat these two situations separately.

4.6.1 Nonlinearities Resulting from Band-to-Band Transitions

For $\hbar\omega > E_g$, the nonlinear response occurs as the result of band-to-band transitions. For all but the shortest laser pulses, the nonlinear response can be described in terms of the conduction band population N_c, which can be taken to obey a rate equation of the form

$$\frac{dN_c}{dt} = \frac{\alpha I}{\hbar\omega} - \frac{(N_c - N_c^{(0)})}{\tau_R}, \tag{4.6.1}$$

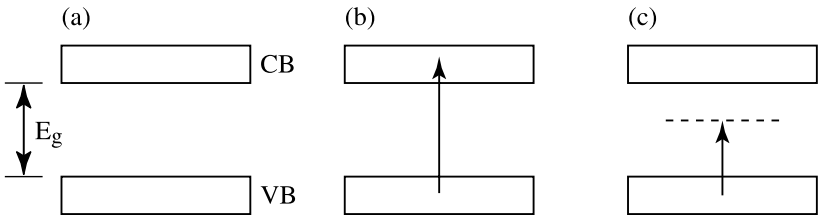

FIGURE 4.6.1: (a) The valence band (VB) and conduction band (CB) of a semiconductor are separated by energy E_g. For $\hbar\omega > E_g$ (b), the nonlinear response results from the transfer of electrons to the conductions band, whereas for $\hbar\omega < E_g$ (c), the nonlinear response involves virtual transitions.

where α is the absorption coefficient of the material at the laser frequency, $N_c^{(0)}$ is the conduction band electron population in thermal equilibrium, and τ_R is the electron–hole recombination time. In steady state this equation possesses the solution

$$N_c = N_c^{(0)} + \frac{\alpha I \tau_R}{\hbar\omega}. \tag{4.6.2}$$

However, for the common situation in which the laser pulse duration is shorter than the material response time τ_R, the conduction-band electron density increases monotonically during the laser pulse.

The change in electron concentration described by Eq. (4.6.1) leads to a change in the optical properties by means of several different mechanisms, which we now describe.

Free-Electron Response

To first approximation, electrons in the conduction band can be considered to respond freely to an applied optical field. The free-electron contribution to the dielectric constant is well known (see, for example, Eq. (13.7.3)) and has the form

$$\epsilon(\omega) = \epsilon_b - \frac{\omega_p^2}{\omega(\omega + i/\tau)}, \tag{4.6.3}$$

where ϵ_b is the contribution to the dielectric constant from bound changes, ω_p^2 is the square of the plasma frequency and is given by $\omega_p^2 = N_c e^2/\epsilon_0 m$, and τ is an optical response time that in general is not equal to τ_R and is typically much shorter than it. Since N_c increases with laser intensity, $\epsilon(\omega)$ is seen to decrease with laser intensity. In the steady-state limit, we can derive an approximate expression (see Problem 11) for the intensity-dependent refractive index as $n = n_0 + n_2 I$, where

$$n_0^2 = \epsilon_b - \frac{N_c(0)e^2}{\epsilon_0 m\omega(\omega + i/\tau)} \tag{4.6.4}$$

and

$$n_2 = -\frac{e^2 \alpha \tau_R}{2\epsilon_b n_0 m \hbar \omega^3}. \tag{4.6.5}$$

Note that n_2 is proportional to ω^{-3}. One thus expects this mechanism to become dominant at long wavelengths. If we evaluate this expression using the characteristic values $m = 0.1\ m_e$ (note that m in Eq. (4.6.5) is the effective mass of the conduction-band electron), $n_0 = 3.5$, $\alpha = 10^4\ \text{cm}^{-1}$, $\hbar\omega = 0.75$ eV, $\tau_r = 10$ nsec, we find that $n_2 = 3 \times 10^{-10}\ \text{m}^2/\text{W}$, a reasonably large value.

Modification of Optical Properties by Plasma Screening Effects

A direct consequence of the presence of electrons in the semiconductor conduction band is that the material becomes weakly conducting. As a result, charges can flow to shield any unbalanced free charges, and the Coulomb interaction between charged particles becomes effectively weakened. In the classical limit in which the electrons obey a Maxwell–Boltzmann distribution, the screened potential energy between two point particles of charge e becomes

$$V(r) = \frac{e^2}{4\pi\epsilon\epsilon_0 r} e^{-\kappa r}, \tag{4.6.6}$$

where ϵ is the (real) dielectric constant of the semiconductor material and where

$$\kappa = \sqrt{\frac{N_c e^2}{\epsilon\epsilon_0 kT}} \tag{4.6.7}$$

is the Debye–Hückel screening wavenumber.

Let us pause here to briefly sketch the derivation of expression (4.6.6) for the screened Coulomb potential. We note that the electrostatic potential $\Phi(\mathbf{r})$ and the total charge density $\rho(\mathbf{r})$ must be related by Poisson's equation

$$\nabla^2 \Phi(\mathbf{r}) = \frac{-1}{\epsilon\epsilon_0} \rho(\mathbf{r}). \tag{4.6.8}$$

We model the semiconductor as an electron plasma, that is, we assume that the electrons are free to move within the material, whereas the positive ions are fixed in position. We assume that the spatial distribution $N_c(\mathbf{r})$ of the conduction-band electrons is determined by the Boltzmann factor, that is, by

$$N_c(\mathbf{r}) = N_{c,0}\, e^{-eV(\mathbf{r})/k_B T}, \tag{4.6.9}$$

where k_B is Boltzmann's constant and T is the kinetic temperature of the electron ensemble. Under homogeneous conditions, the potential $\Phi(\mathbf{r})$ and electron density $N_c(\mathbf{r})$ become spatially uniform. Let us now assume that a point charge Q (assumed positive for definiteness) is

introduced into the system and placed at the origin of the coordinate system. Electrons will be drawn toward Q, with the effect of decreasing the field created by Q when measured at large distances. Closer to Q, the shielding will not be complete. We now estimate the form of the potential distribution in the vicinity of Q. The total charge density is now given by

$$\rho(\mathbf{r}) = Q\delta(\mathbf{r}) - e\,\Delta N_c(\mathbf{r}), \tag{4.6.10}$$

where $\delta(\mathbf{r})$ is the Dirac delta function and where $\Delta N_c(\mathbf{r})$ is the change in the electron distribution induced by the reaction to the point charge Q. We see by expanding Eq. (4.6.9) in a power series in $V(\mathbf{r})$ that to first order in the potential the quantity $\Delta N_c(\mathbf{r})$ is given by

$$\Delta N_c(\mathbf{r}) = -N_{c,0}\, eV(\mathbf{r})/k_B T. \tag{4.6.11}$$

Eqs. (4.6.10) and (4.6.11) are now introduced into Poisson's equation (4.6.8), which can then be rewritten as

$$(\nabla^2 - \kappa^2)\Phi(\mathbf{r}) = \frac{-1}{\epsilon\epsilon_0} Q\delta(\mathbf{r}), \tag{4.6.12}$$

where we have introduced the Debye–Hückel screening wavenumber

$$\kappa = \sqrt{\frac{N_c e^2}{\epsilon\epsilon_0 kT}}. \tag{4.6.13}$$

The inverse of this quantity is known as the Debye length

$$\lambda_D = 1/\kappa = \sqrt{\frac{\epsilon\epsilon_0 kT}{N_c e^2}}. \tag{4.6.14}$$

The Debye length defines the distance scale over which electrostatic forces are important in a material medium. Eq. (4.6.12) can readily be solved to provide the form of the screened Coulomb potential. One finds that

$$\Phi(r) = \frac{-e}{4\pi\epsilon\epsilon_0 r} e^{-\kappa r}, \tag{4.6.15}$$

Eq. (4.6.6), quoted above, follows from this result by noting that $V(r) = -e\Phi(r)$.

One consequence of the reduction of the strength of the Coulomb interaction is that excitonic features can disappear at high conduction-band electron densities. Let us recall briefly the nature of excitonic features in semiconductors. An electron in the conduction band will feel a force of attraction to a hole in the valence band as the result of their Coulomb interaction. This

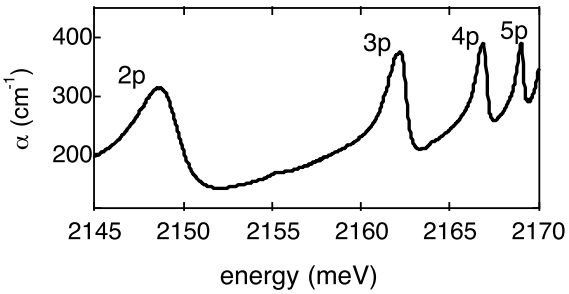

FIGURE 4.6.2: Absorption spectrum of Cu_2O at a temperature of 4.2 K. The spectral features result from transitions from the top of the valence band to the exciton level labeled in the figure. (After Tayagaki et al., 2005.)

attraction can be sufficiently strong that the pair forms a bound state known as an exciton. Excitonic energy levels typically lie slightly below the edge of the conduction band, at an energy given by

$$E_n = E_c - R^*/n^2, \tag{4.6.16}$$

where n is the principal quantum number, E_c is the energy of the bottom of the conduction band, and $R^* = \hbar^2(2m_r a_0^{*2})^{-1}$ is the effective Rydberg constant. Here m_r is the reduced mass of the electron–hole pair and $a_0^* = 4\pi\epsilon_0\hbar^2(m_r e^2)^{-1}$ is the effective first Bohr radius. Laboratory results showing absorption features associated with transitions to these excitonic levels are shown in Fig. 4.6.2. Often only the lowest exciton states contribute significantly to the semiconductor absorption spectrum. The situation in which only the $n = 1$ state contributes is shown in the conceptual sketch of Fig. 4.6.3(a). In the presence of a laser beam sufficiently intense to place an appreciable population of electrons into the conduction band, plasma screening effects can lead to the disappearance of these excitonic resonances, leading to an absorption spectrum of the sort shown in part (b) of the figure. Let $\Delta\alpha$ denote the amount by which the absorption coefficient has changed because of the presence of the optical field. The change in absorption coefficient is accompanied by a change in refractive index. This change can be calculated by means of the Kramers–Kronig relations (see Section 1.7), which in the present context we write in the form

$$\Delta n(\omega) = \frac{c}{\pi}\int_0^\infty \frac{\Delta\alpha(\omega')\,d\omega'}{\omega'^2 - \omega^2}, \tag{4.6.17}$$

where the principal part of the integral is to be taken. The change in refractive index is shown symbolically in part (c) of Fig. 4.6.3. Note that Δn is positive on the high-frequency side of the exciton resonance and is negative on the low-frequency side. However, the change in refractive index is appreciable only over a narrow range of frequency on either side of the exact resonance.

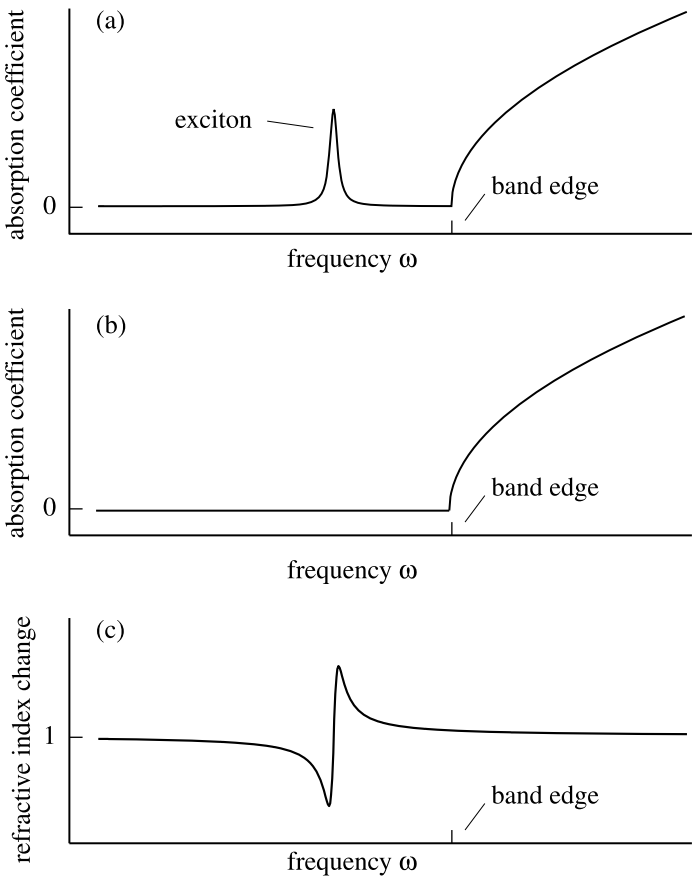

FIGURE 4.6.3: Schematic low-temperature absorption spectrum of a semiconductor in the absence (a) and in the presence (b) of an appreciable number of optically excited conduction band electrons. (c) The modification of the refractive index associated with the optically induced change in absorption coefficient.

Change of Optical Properties Due to Band-Filling Effects

As electrons are transferred from the valence band to the conduction band, the absorption coefficient of a semiconductor must decrease. This effect is in many ways analogous to saturation effects in atomic systems, as described in Chapter 6, but in the present case with the added complexity that the electrons must obey the Pauli principle and thus must occupy a range of energies within the conduction band. This process leads to a lowering of the refractive index for frequencies below the band edge and a raising of the refractive index for frequencies above the band edge. The sense of the change in refractive index is thus the same as that for a two-level atom. The change in refractive index resulting from band filling can be calculated more pre-

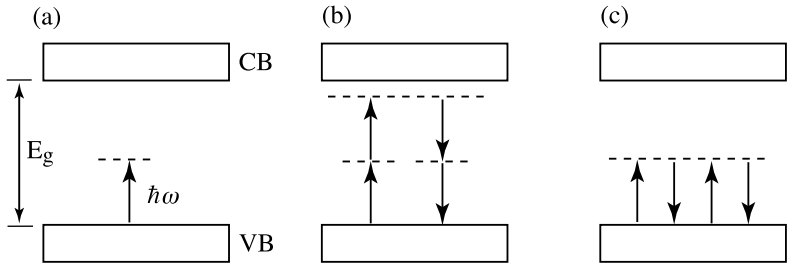

FIGURE 4.6.4: (a) For $\hbar\omega < E_g$, the nonlinear response involves virtual transitions. Under many circumstances, virtual two-photon processes (b) make a larger contribution to the nonlinear response than do one-photon processes (c).

cisely by means of a Kramers–Kronig analysis of the sort described in the previous paragraph; details are described, for instance, by Peyghambarian et al. (1993, Section 13-4).

Change in Optical Properties Due to Band-Gap Renormalization

For reasons that are rather subtle (exchange and Coulomb correlations), the band-gap energy of most semiconductors decreases at high concentrations of conduction band electrons, with a resulting change in the optical properties.

4.6.2 Nonlinearities Involving Virtual Transitions

Let us next consider the nonlinear response of a semiconductor or insulator under the condition $\hbar\omega < E_g$, as illustrated in Fig. 4.6.4(a). In this situation, the photon energy is too small to allow single-photon absorption to populate the conduction band, and the nonlinear response involves virtual processes such as those shown in parts (b) and (c) of the figure. The "two-photon" process of part (b) usually is much stronger than the "one-photon" process of part (c) except for photon energies $\hbar\omega$ approaching the band-gap energy E_g. In the approximation in which only the two-photon process of part (b) is considered, a simple model can be developed to describe the nonlinear response of the material. We shall not present the details here, which involve some considerations of the band theory of solids that lie outside the scope of the present work. Sheik-Bahae et al. (1990, 1991) have addressed this problem theoretically and have shown that the dominant contribution to the imaginary part of the nonlinear response is the two-photon absorption process shown in Fig. 4.6.4(b). The real part of the nonlinear response is then obtained through a Kramers–Kronig transform of the imaginary part. Specifically, they find that the real part of the nonlinear refractive index coefficient defined such that $\Delta n = n_2 I$ can be expressed

as

$$n_2 = K\frac{\hbar c\sqrt{E_p}}{2n_0^2 E_g^4} G_2(\hbar\omega/E_g), \tag{4.6.18}$$

where $E_p = 21$ eV, K can be considered to be a single free parameter whose value is found empirically to be 3.1×10^3 in units such that E_p and E_g are measured in eV and n_2 is measured in cm^2/W, and where G_2 is the universal function

$$G_2(x) = \frac{-2 + 6x - 3x^2 - x^3 - \frac{3}{4}x^4 - \frac{3}{4}x^5 + 2(1-2x)^{3/2}\Theta(1-2x)}{64x^6}, \tag{4.6.19}$$

where $\Theta(y)$ is the Heaviside step function defined such that $\Theta(y) = 0$ for $y < 0$ and $\Theta(y) = 1$ for $y \geq 0$. In the same approximation, the two-photon absorption coefficient defined such that $\alpha = \alpha_0 + \beta I$ is given by

$$\beta = \frac{K\sqrt{E_p}}{n_0^2 E_g^3} F_2(2\hbar\omega/E_g), \tag{4.6.20}$$

where F_2 is the universal function

$$F_2(2x) = \frac{(2x-1)^{3/2}}{(2x)^5} \quad \text{for} \quad 2x > 1 \tag{4.6.21}$$

and $F_2(2x) = 0$ otherwise. These functional forms are illustrated in Fig. 4.6.5. Note that the process of two-photon absorption vanishes for $\hbar\omega < \frac{1}{2}E_g$ for reasons of energetics. Note also that the nonlinear refractive index peaks at $\hbar\omega/E_g \approx 0.54$, vanishes at $\hbar\omega/E_g \approx 0.69$, and is negative for $\hbar\omega/E_g \gtrsim 0.69$. Note also from Eq. (4.6.18) that n_2 scales as E_g^{-4}. Thus narrow-band-gap semiconductors are expected to produce a much larger nonlinear response than large-band-gap semiconductors. These predictions are in very good agreement with experimental results; see, for instance, Fig. 4.6.6. In plotting this figure, some additional contributions to the nonlinear response not included in Eqs. (4.6.18) through (4.6.21), such as the Raman effect and linear and quadratic Stark effects, have been included in the prediction (Sheik-Bahae et al., 1991).

In general, both the slow, band-to-band nonlinearities considered earlier and the instantaneous nonlinearities considered here occur simultaneously. Said et al. (1992) have studied several semiconductors under conditions such that both processes occur simultaneously, and they find that the change in refractive index is well described by the equation

$$\Delta n = n_2 I + \sigma_r N_c, \tag{4.6.22}$$

where as usual n_2 gives the instantaneous nonlinear response and where σ_r is the change in refractive index per unit conduction band electron density. Their measured values of these quantities as well as the two-photon-absorption coefficient are given in Table 4.6.1.

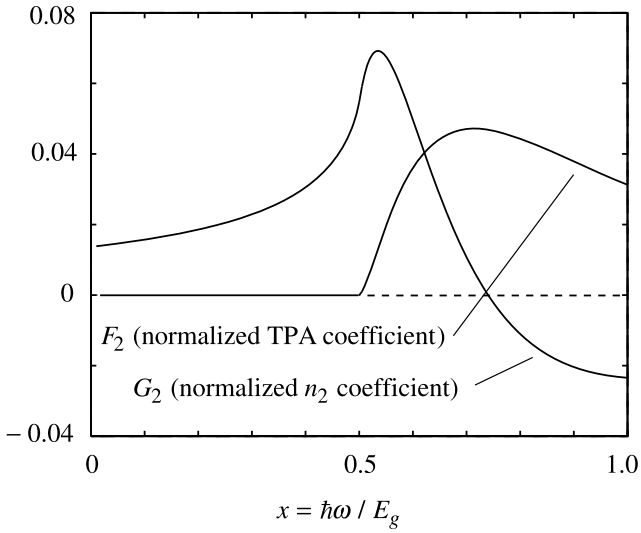

FIGURE 4.6.5: Variation of the nonlinear refraction coefficient n_2 and the two-photon-absorption coefficient with photon energy $\hbar\omega$ according to the model of Sheik-Bahae et al. (1990).

TABLE 4.6.1: Nonlinear optical coefficients of several semiconductors.

Semiconductor	β (m/TW)	n_2 (m^2/W)	σ_r (m^3)
ZnSe at 532 nm	58	-6.8×10^{-18}	-0.8×10^{-27}
GaAs at 1064 nm	260	-4.1×10^{-17}	-6.5×10^{-27}
CdTe at 1064 nm	260	-3×10^{-17}	-5×10^{-27}
ZnTe at 1064 nm	42	1.2×10^{-17}	-0.75×10^{-27}

After Said et al. (1992).

4.7 Concluding Remarks

Throughout this chapter, we have assumed that the refractive index variation Δn scales monotonically with laser intensity as $\Delta n = n_2 I$. In fact, for any given material there is a maximum change in refractive index that can be observed. This maximum index change comes about either because of saturation effects or because there is a maximum laser intensity that can be used in order to avoid laser damage effects. A particularly large value of the refractive index variation of $\Delta n_{\max} = 0.14$ has been reported by Brzozowski et al. (2003). This large change was observed in an InGaAs/InAlGaAs multiple quantum well sample at a wavelength of approximately 1500 nm and using a pulse fluence of 116 $\mu J/cm^2$. Quite recently, even larger values have been reported. Alam et al. (2016) report the value $\Delta n_{\max} = 0.7$ in indium tin oxide, and Caspani et al. (2016) report the value $\Delta n_{\max} = 4.4$ in aluminum-zinc oxide.

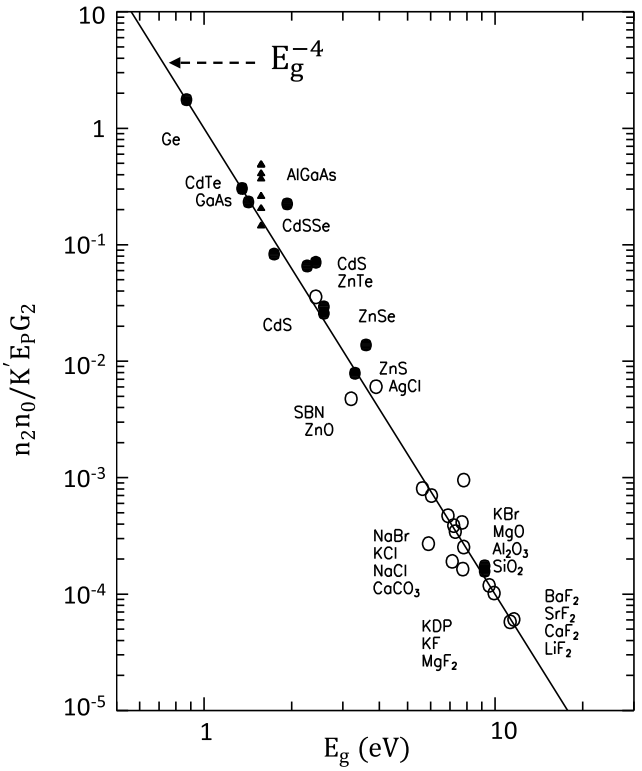

FIGURE 4.6.6: Comparison of the predictions (solid line) of the model of Sheik-Bahae et al. (1991) with measured values (data points) of the nonlinear refraction parameter n_2 for a variety of materials.

For certain conceptual purposes, it can be useful to express the nonlinear susceptibility in dimensionless form (see, for instance, Kok et al. (2002)). One prescription for doing so is to define the dimensionless susceptibility as

$$\chi_{\mathrm{D}}^{(3)} = E_{1,\max}^2 \chi^{(3)}, \tag{4.7.1}$$

where $E_{1,\max}^2$ is the largest electric field that can be produced in free space by a single photon. Since a pulse of light can be localized to a volume of the order the cube of the vacuum wavelength λ, one finds that

$$\frac{\hbar\omega}{\lambda^3} = 2\epsilon_0 E_{1,\max}^2 \tag{4.7.2}$$

and thus that

$$\chi_{\mathrm{D}}^{(3)} = \frac{\hbar\omega}{2\epsilon_0 \lambda^3} \chi^{(3)}. \tag{4.7.3}$$

For the case of fused silica ($\chi^{(3)} = 2.5 \times 10^{-22}$ m^2/W^2) and a wavelength of 1.0 μm, this expression for the dimensionless nonlinear suscpetibility becomes when evaluated becomes $\chi_D^{(3)} = 4.5 \times 10^{-13}$. This number can be taken to represent a typical value of $\chi_D^{(3)}$. The smallness of this number quantifies the notion that nonresonant nonlinear optical interactions tend to be extremely weak, at least on a local scale. It is only the cumulative effect of nonlinear interactions taking place over large distances that allows nonlinear processes to produce intense output fields. It should be noted, however, that for some of the largest reported optical nonlinearities the dimensionless susceptibility can become large. For example, for the case of the nonlinear response of a Bose–Einstein condensate, as quoted in Table 4.1.2, the dimensionless susceptibility becomes $\chi_D^{(3)} \approx 100$.

Problems

1. *n_2 for a lossy medium.* Generalize the derivation of Eq. (4.1.19) to allow the linear refractive index to be a complex quantity $\bar{n}_0$.
   [Ans: Replace n_0^2 in the denominator of Eq. (4.1.19) by $\bar{n}_0 \operatorname{Re} \bar{n}_0$.]
2. *Tensor properties of $\chi^{(3)}$ for an isotropic medium.* Derive Eqs. (4.2.2).
3. *Ellipse rotation.* A 1-cm-long sample of carbon disulfide is illuminated by elliptically polarized light of intensity $I = 1$ MW/cm^2. Determine how the angle through which the polarization ellipse is rotated depends upon the ellipticity of the light, and calculate numerically the maximum value of the rotation angle. Quantify the ellipticity in terms of the parameter δ where $(-1 \leq \delta \leq 1)$ which defines the polarization unit vector through the relation
$$\hat{\boldsymbol{\epsilon}} = \frac{\hat{\mathbf{x}} + i\delta\hat{\mathbf{y}}}{(1+\delta^2)^{1/2}}.$$
   [Hint: The third-order nonlinear optical response of carbon disulfide is due mainly to molecular orientation.]
4. *Sign of $\chi^{(3)}$.* Verify the statement made in the text that the first term in expression (4.3.12) is positive whenever ω is smaller than any resonance frequency of the atomic system.
5. *Tensor properties of the molecular orientation effect.* Derive the result given by Eqs. (4.4.27) through (4.4.30) for the general case in which a, b, and c are all distinct.
   [This problem is extremely challenging.]
6. *Thermal nonlinearities.* In Section 4.5, we basically used dimensional analysis to make an order-of-magnitude estimate of the size of thermal nonlinearities. In this problem, we consider a situation in which the equation of heat transport can be solved exactly.
   Consider a laser beam of diameter D_1 and power P propagating through a long glass rod of diameter D_2. The outer surface of the glass rod is held at the fixed temperature T_0. Assume steady-state conditions, and make the simplifying assumption that the transverse

intensity profile of the laser beam is uniform. Determine the local temperature T at each point within the glass rod and determine the maximum change in refractive index. Evaluate numerically for realistic conditions.

7. *Nonlinearity due to the magnetic force.* Consider a plane electromagnetic wave incident upon a free electron. If the field is strong enough, the electron will acquire sufficient velocity that the magnetic force $\mathbf{F}_M = (-e/c)\mathbf{v} \times \mathbf{B}$ has a noticeable effect on its motion. This is one source of the nonlinear electronic response.
(a) Show that for an optical plane wave with electric field $\mathbf{E} = \hat{\mathbf{x}}\,(E_0 e^{i(kz-\omega t)} + \text{c.c.})$ the electromagnetic force on an electron is

$$\mathbf{F}_{EM} = -e\big(E_0 e^{-i\omega t} + \text{c.c.}\big)\left[\hat{\mathbf{x}}\left(1 - \frac{\dot{z}}{c}\right) + \hat{\mathbf{z}}\left(\frac{\dot{x}}{c}\right)\right].$$

How large (order of magnitude) can $\dot{x}/c$ become for a free electron in a beam with a peak intensity of 10^{17} W/cm^2?
(b) Derive expressions for $\chi^{(2)}(2\omega)$ and $\chi^{(2)}(0)$ for a collection of free electrons in terms of the electron number density N. (You may assume there are no "frictional" forces.) In what direction(s) will light at 2ω be emitted?
(c) Derive expressions for $\chi^{(3)}(\omega)$ and $\chi^{(3)}(3\omega)$.
(d) Good conductors can often be modeled using the free electron model. Assuming the magnetic force is the only source of optical nonlinearity, make a numerical estimate (order of magnitude) of $\chi^{(3)}(\omega)$ for gold.

8. *Nonlinear phase shift of a focused gaussian beam.* Derive an expression for the nonlinear phase shift experienced by a focused gaussian laser beam of beam-waist radius w_0 carrying power $\mathcal{P}$ in passing through a nonlinear optical material characterized by a nonlinear refractive index n_2. Perform this calculation by integrating the on-axis intensity from $z = -\infty$ to $z = +\infty$. Comment on the accuracy of this method of calculation, and speculate regarding computational methods that could provide a more accurate prediction of the nonlinear phase shift.

9. *Nonlinear phase shift of a focused gaussian beam.* Assuming the validity of the procedure used in the previous question (that is, by integrating from $-\infty$ to $+\infty$), determine numerically the nonlinear phase shift that can be obtained by a focused gaussian laser beam in propagating through optical glass, when the power of the beam is adjusted to be just below the laser damage threshold. Assume initially that the glass is a plate 1 cm thick, but also describe how the phase shift scales with the thickness of the glass plate. For definiteness, assume that the beam waist is at the center of the glass block, and assume that bulk (not surface) damage is the limiting process. Take $I\,(\text{damage}) = 10$ GW/cm^2.

10. *Nonlinear phase shift of a focused gaussian beam.* Same as the previous problem, but assume that surface damage is the limiting process.

11. *Semiconductor nonlinear response.* Derive Eq. (4.6.5).

References

General References

Alam, M.Z., De Leon, I., Boyd, R.W., 2016. Science 352, 795–797.

Chiao, R.Y., Kelley, P.L., Garmire, E., 1966. Phys. Rev. Lett. 17, 1158.

Close, D.H., Giuliano, C.R., Hellwarth, R.W., Hess, L.D., McClung, F.J., 1966. IEEE J. Quantum Electron 2, 553.

Hanna, D.C., Yuratich, M.A., Cotter, D., 1979. Nonlinear Optics of Free Atoms and Molecules. Springer-Verlag, Berlin.

Hellwarth, R.W., 1977. Prog. Quantum Electron. 5, 1–68.

Orr, B.J., Ward, J.F., 1971. Mol. Phys. 20, 513.

Recommended Additional Reading

Brewer, R.G., Lifshitz, J.R., Garmire, E., Chiao, R.Y., Townes, C.H., 1968. Phys. Rev. 166, 326.

Carman, R.L., Chiao, R.Y., Kelley, P.L., 1966. Phys. Rev. Lett. 17, 1281.

Chiao, R.Y., Godine, J., 1969. Phys. Rev. 185, 430.

Landauer, R., 1967. Phys. Lett. A 25, 416.

Owyoung, A., 1971. The Origins of the Nonlinear Refractive Indices of Liquids and Glasses. Ph.D. dissertation. California Institute of Technology.

Svelto, O., 1974. In: Wolf, E. (Ed.), Progress in Optics VII. North Holland, Amsterdam.

Tensor Nature of the Third-Order Susceptibility

Butcher, P.N., 1965. Nonlinear Optical Phenomena. Ohio State University.

Gaeta, A.L., Boyd, R.W., Ackerhalt, J.R., Milonni, P.W., 1987. Phys. Rev. Lett. 58, 2432.

Gauthier, D.J., Malcuit, M.S., Boyd, R.W., 1988. Phys. Rev. Lett. 61, 1827.

Gauthier, D.J., Malcuit, M.S., Gaeta, A.L., Boyd, R.W., 1990. Phys. Rev. Lett. 64, 1721.

Maker, P.D., Terhune, R.W., 1965. Phys. Rev. 137, A801.

Maker, P.D., Terhune, R.W., Savage, C.M., 1964. Phys. Rev. Lett. 12, 507.

Saikan, S., Kiguchi, M., 1982. Opt. Lett. 7, 555.

Thermal Nonlinear Optical Effects

Bentley, S.J., Boyd, R.W., Butler, W.E., Melissinos, A.C., 2000. Opt. Lett. 25, 1192.

Bespalov, V.I., Betin, A.A., Zhukov, E.A., Mitropol'sky, O.V., Rusov, N.Y., 1989. IEEE J. Quantum Electron. 25, 360.

Hoffman, H.J., 1986. J. Opt. Soc. Am. B 3, 253.

Martin, G., Hellwarth, R.W., 1979. Appl. Phys. Lett. 34, 371.

Tochio, J.O., Sibbett, W., Bradley, D.J., 1981. Opt. Commun. 37, 67.

Semiconductor Nonlinearities

Peyghambarian, N., Koch, S.W., Mysyrowicz, A., 1993. Introduction to Semiconductor Optics. Prentice Hall, Englewood Cliffs, NJ.

Said, A.A., Sheik-Bahae, M., Hagan, D.J., Wei, T.H., Wang, J., Young, J., Van Stryland, E.W., 1992. J. Opt. Soc. Am. B 9, 405.

Sheik-Bahae, M., Hagan, D.J., Van Stryland, E.W., 1990. Phys. Rev. Lett. 65, 96.

Sheik-Bahae, M., Hutchings, D.C., Hagan, D.J., Van Stryland, E.W., 1991. IEEE J. Quantum Electron. 27, 1296.

Tayagaki, T., Mysyrowicz, M., Kuwata-Gonokami, M., 2005. J. Physical Society of Japan 74, 1423.

Recommended Additional Reading

Butcher, P.N., Cotter, D., 1990. The Elements of Nonlinear Optics. Cambridge University Press, Cambridge, UK, Chapter 8.

Debye, P., Hückel, E., 1923. Physikalische Zeitschrift. 24, 185–206.

Hache, F., Ricard, D., Flytzanis, C., Kreibig, U., 1988. Appl. Phys. A 47, 347.

Peyghambarian, N., Koch, S.W., 1990. In: Gibbs, H.M., Khitrova, G., Peyghambarian, N. (Eds.), Nonlinear Photonics. In: Springer Series in Electronics and Photonics, vol. 30.

Weber, M.J. (Ed.), 1995. CRC Handbook of Laser Science and Technology, Supplement 2, Optical Materials. CRC Press, Boca Raton, FL, Chapter 8.

Concluding Remarks

Brzozowski, L., Sargent, E.H., Thorpe, A.S., Extavour, M., 2003. Appl. Phys. Lett. 82, 4429.

Caspani, L., Kaipurath, R.P.M., Clerici, M., Ferrera, M., Roger, T., Kim, J., Kinsey, N., Pietrzyk, M., Di Falco, A., Shalaev, V.M., Boltasseva, A., Faccio, D., 2016. Phys. Rev. Lett. 116, 233901.

Kok, P., Lee, H., Dowling, J.P., 2002. Phys. Rev. A 66, 063814.